UNIVERSITA' DEGLI STUDI DI PALERMO

Dipartimento di Fisica e Chimica
Dottorato Di Ricerca In Fisica Applicata – XXIV Ciclo

A physical – computational modelling for analysis of Centromere patterns in IIF images

A thesis by:
Letizia Vivona

Tutor:
Prof. Giuseppe Raso

Coordinator:
Prof. Bernardo Spagnolo

SSD: FIS/07

Contents

Introduction

Autoimmune diseases are a family of more than 80 chronic, and often disabling, illnesses that develop when underlying defects in the immune system lead the body to attack its own organs, tissues, and cells.

Diagnosing autoimmune diseases can be particularly difficult because these disorders can affect any organ or tissue in the body, and produce highly diverse clinical manifestations, depending on the site of autoimmune attack. Moreover, disease symptoms are often not apparent until the disease has reached a relatively advanced stage.

Laboratory's techniques able to point out and confirm diagnosis of autoimmune pathologies are based on research and identification of autoantibodies, revealed by the presence of specific antigen- antibody complexes. Particularly, identification of antinuclear antibodies (ANA) through indirect immunofluorescence (IIF) method is an important part of clinical medicine and clinical immunology. The classification is based on fluorescence intensity and pattern recognition. Although the IIF techniques have increased progressively since immunofluorescence techniques were first used to demonstrate antinuclear antibodies in 1957, there are still various disadvantages in these techniques, among them the lack of an automatic procedures which could make easier, faster and more reliable the tests execution and lower costs.

These observation suggested to develop an automated method to support the IIF diagnosis, expecting advantages also in the reduction of false negative and false positive results.

Developing an automated procedure for diagnosis of autoimmune diseases, generally authors focus their attention on cells detection, fluorescence intensity determination or staining pattern classification. Since the presence of antibodies against antigens in different location determines different patterns of fluorescence, we chosen to deal with the IIF pattern recognition because different patterns correspond to different diseases, so it is really important to be able to distinguish among different pattern. In the literature, the principal staining patterns are classified into one of the following groups:

- homogeneous: diffuse staining of the interphase nuclei and staining of the chromatin of mitotic cells;
- speckled: a fine or coarse granular nuclear staining of the interphase cell nuclei;
- nucleolar: large coarse speckled staining within the nucleus, less than six in number per cell;
- cytoplasmic: fine fluorescent fibres running the length of the cell; it is frequently associated with other autoantibodies to give a mixed pattern;
- centromere: several discrete speckles distributed throughout the interphase nuclei and characteristically found in the condensed nuclear chromatin during mitosis as a bar of closely associated speckles.

Among this pattern, the centromere pattern has been only partially investigated because, according to the literature, it does not show well-defined cell edges and the high variability of fluorescence intensity inside the centromere cells makes a difficult task the application of segmentation procedures. Nevertheless, it is known that a centromere cell contains small bright dots inside a weakly fluorescent nucleus, so an expertise may recognize a centromere pattern by only counting the fluorescent centromeres.

For these reasons, since a CAD systems should reproduce the human eye response, we propose here a method to automatically classify the centromere pattern based on the grouping of centromeres present on the cells through a clustering algorithm.

In this respect, the first chapter is dedicated to the description of automatic systems for supporting in early diagnosis, to the description of the autoimmune diseases and to the state of the art regarding the method of classifications.

In the second chapter it is described the project A.I.D.A. inside which this thesis is inserted and the database used to test the algorithm; the characteristics of the algorithm are described too, with a paragraph dedicated to clustering algorithm. In the second chapter there is also a paragraph dedicated to the description of the figures of merit used to verify the properties of the algorithm and a paragraph dedicated to the description of a public database also used for testing the proposed method.

The third chapter is dedicated to the description of the various phases of developing of the algorithm and to the presentation and discussion of the experimental results.

Chapter 1

1.1 The expert systems

Studies indicate that, in medical imaging, the radiologists often do not detect all abnormalities on images that are visible on retrospective review, and they do not always correctly characterize abnormalities that are found.

Techniques developed in computer vision and automated pattern recognition can be applied to assist radiologists in reading images: the computer manipulates a digital image bringing the suspicious regions to the attention of radiologists. So, radiologists can use the computer as a second opinion, or as a pointer to suspicious regions. This may increase the accuracy of screening programs, and it may avoid the need of double reading [1].

Although early attempts at computerized analysis of medical images were made in the 1960s, serious and systematic investigation on Computer – Aided Device or Computer- Aided Detection (CAD) systems began in the 1980s with a fundamental change in the concept for utilization of the computer output, from automated computer diagnosis to computer-aided diagnosis.

A CAD system allows to reduce the noise in the image, to improve the contrast among a region of interest (ROI) and background and to extract and select the characteristics of the ROI and progress to a correct classification. To determine if an area on an image looks suspicious, a CAD system divides the problem into various components [2]: a general scheme of a CAD system is shown in Figure 1.1.

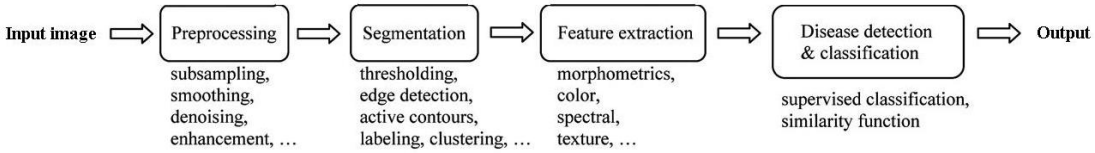

Figure 1.1: Example of CAD system

The goal of ***preprocessing*** is removing differences between data from different sources or obtained with different protocols. Scanned images need to be calibrated, data may have to be resampled to a fixed resolution, and many techniques can be applied to enhance the image [2] ─ [6]. Removing blurring and noise, increasing contrast, and revealing details are examples of enhancement operations. The enhancement techniques differ from one field to another according to their objective. The existing techniques of image enhancement can be classified into two categories: *Spatial Domain* and *Frequency Domain* enhancement. In Spatial Domain techniques, like the logarithmic transforms, power law transforms, histogram equalization, pixel values are manipulated to achieve desired enhancement. In Frequency Domain methods, the Fourier Transform of the image is first computed. All the enhancement operations are performed on the Fourier transform of the image and then the Inverse Fourier transform is performed to get the resultant image [7]-[9].

The second step of a CAD system is ***segmentation***, i.e. the division of an image I in S_I not-overlapped regions, each of them being homogeneous and uniform compared to some features. An incomplete segmentation can make CAD systems lost information in the unsegmented areas. Segmentation of nontrivial images is one of the most difficult tasks in image processing and segmentation accuracy determines the eventual success or failure of the overall computerized analysis procedures [2].

Segmentation techniques developed during this years are numerous and very different among them. Basically, the segmentation is divided in two categories: *region-based segmentation* and *edge-based segmentation* [10]-[13].

The region-based techniques produce coherent regions. All pixels in a coherent region are supposed similar with respect to some characteristic or computed property, such as colour, intensity, or texture. Adjacent regions are supposed significantly different with respect to the same characteristics. For grey-level images, the most basic

attribute used is the luminance amplitude (grey level), so it is possible to separate luminous regions from background performing a thresholding operation. In this way, any pixel (x, y) is selected as a part of foreground if its intensity is higher than or equal to a threshold value, i.e. $f(x, y) \geq T$, else pixels points to background.

The problems in thresholding are the correct determination of a threshold (usually, a method used to select T is by observing histograms of particular image considered for segmentation) and that pixels with analogous grey level may not be adjacent.

Another region-based method is region growing [14]: suppose that we start with a single pixel *p* and we wish to expand from that seed pixel to fill a coherent region. We can define a similarity measure $S(i, j)$ such that it produces a high result if pixels *i* and *j* are similar and a low one otherwise. First, consider a pixel *q* adjacent to the pixel *p*. We can add pixel *q* to pixel *p*'s region if $S(p, q) > T$ for some threshold T. We can then proceed to the other neighbours of *p* and do likewise. Suppose that $S(p, q) > T$ and we added pixel *q* to pixel *p*'s region. We can now similarly consider the neighbours of *q* and add them likewise if they are similar enough.

The edge-based segmentation techniques are based on searching pixels that constitute the contour of the objects, individualized in correspondence of discontinuity in grey level; pixels of contour are joined to form a closed line delimiting a region. Pixels not included will be considered belonging to background.

Other segmentation techniques use fractal models [15] ─ [17], or wavelet transforms [18], [19].

After the segmentation, a number of regions of interest (ROI) are identified that merit further attention by radiologists. For every ROI it is possible to define a set of characteristics, called features, used to classify the regions.

The ***features extraction*** is a crucial step in a CAD system because now each ROI is represented by a vector, a row of numbers, one for each feature. The feature vector can be represented geometrically by a point in a feature space. This feature space has a dimension that is identical to the number of features [2].

Features are extracted from the first-order grey-level histogram, defined as the distribution of the probability of occurrence of a grey-level in the image, and from the second-order histogram, $H(y_q, y_r, d)$, which represents the distribution of probability of

occurrence of a pair of grey level values separated by a given displacement vector *d* [3], [4].

If P(*b*) is the probability of occurrence of a certain grey level *b*, it is possible to define the following list of features:

Mean	$\sum_{b=0}^{L-1} bP(b)$
Standard Deviation	$\sqrt{\sum_{b=0}^{L-1} (b-\bar{b})^2 P(b)}$
Skewness	$\frac{\sum_{b=0}^{L-1} (b-\bar{b})^3 P(b)}{\sigma^3}$
Kurtosis	$\frac{\sum_{b=0}^{L-1} (b-\bar{b})^4 P(b)}{\sigma^4}$
Energy	$\sum_{b=0}^{L-1} P(b)^2$
Entropy	$-\sum_{b=0}^{L-1} P(b)\log_2 P(b)$

If P(*a*, *b*) is the joint probability of occurrence of a pixel *a* near a pixel *b* it is possible to define the following list of features:

Autocorrelation	$\sum_{a=0}^{L-1}\sum_{b=0}^{L-1} abP(a,b)$
Covariance	$\sum_{a=0}^{L-1}\sum_{b=0}^{L-1} (a-\bar{a})(b-\bar{b})P(a,b)$
Inertia	$\sum_{a=0}^{L-1}\sum_{b=0}^{L-1} (a-b)^2 P(a,b)$
Absolute value	$\sum_{a=0}^{L-1}\sum_{b=0}^{L-1} \lvert a-b\rvert P(a,b)$
Inverse Difference	$\sum_{a=0}^{L-1}\sum_{b=0}^{L-1} \frac{P(a,b)}{1+(a-b)^2}$

Co-Energy $$\sum_{a=0}^{L-1}\sum_{b=0}^{L-1} P(a,b)^2$$

Co-Entropy $$-\sum_{a=0}^{L-1}\sum_{b=0}^{L-1} P(a,b)\log_2 P(a,b)$$

After the segmentation and the features extraction phases, the problem of identifying regions in feature space is solved by ***classification*** phase. There is no single best technique for classification: neural networks, support vector machines and Bayesian techniques are all mathematical models that may or may not work well depending on the task at hand. CAD researchers therefore always experiment with several classifiers [2], [20].

Neural networks ([21] ─ [26]), for example, reproduce biological neurons (Figure 1.2) which represent the elementary unity of a nervous biological system. Neurons are organized in structures in which they can cooperate for resolving complex problems.

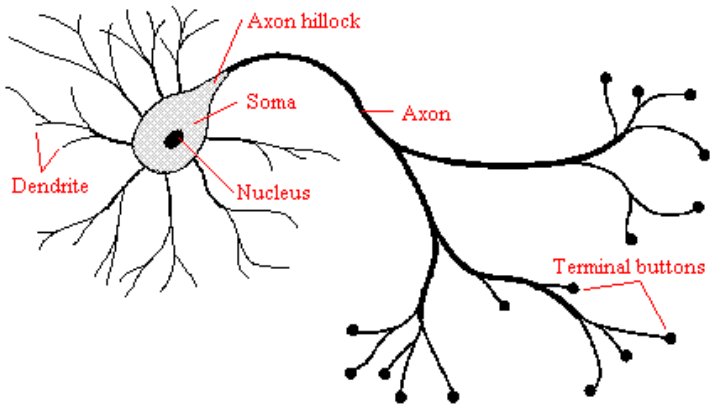

Figure 1.2: Schematic of biological neuron

The dendrites receive the electric impulses from the others neurons through biochemists processes. According to the chemical nature of the synapses, every junction can amplify or reduce the transmitted signal. If the sum of all the electric signals in input overcomes a threshold, the neuron transmits the signal to the other connected neurons through the going out (*axon*) fibre. After the activation, the neuron has a dead time during which it doesn't receive and it doesn't transmit signals.

First mathematic definition of artificial neuron was made in 1943 by McCulloch e Pitt [27]. Input signals at time t, $x_1(t)$, $x_2(t)$,…$x_n(t)$, coming from other neurons are

supposed to be binary and transmitted through synapses to the cell body. Biological effect of synapses is mathematically realized by different weights given to input signals. Neuron input *a*(t) is the sum of all input signals conveniently weighted:

$$a(t)=w_1 x_1(t)+w_2 x_2(t)+\ldots..w_n x_n(t) \qquad (1.1.1)$$

A step function *f*(a) set the output *o*(t+1) at 0 (inactive neuron) or at 1 (active neuron), if *a*(t) overcomes or not the threshold (Figure 1.3).

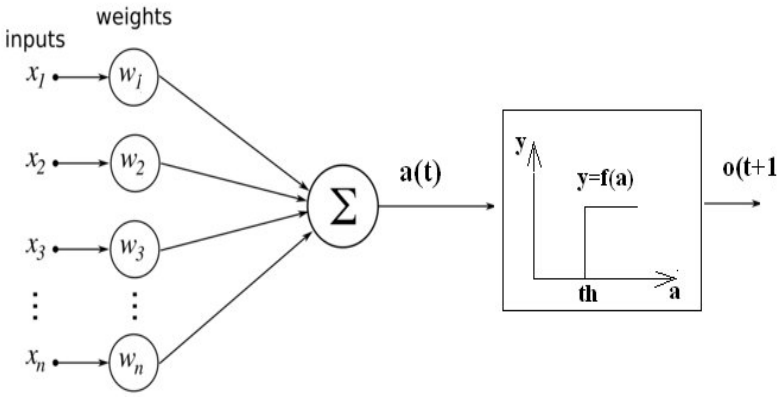

Figure 1.3: Schematic of artificial neuron

The output signal, according to McCulloch e Pitt, is:

$$o(t+1)=f\left(\sum_{i=1}^{n} w_i x_i(t)\right) \qquad (1.1.2)$$

The simplest neural network has a unidirectional connection forward and only one layer of artificial neuron, and the outputs are the same number of the inputs.

In solving more complex problems it is possible to increase the neurons layers, so the first layer pre-process the input and the following layers, called hidden layers, are capable of extracting higher order statistics, discriminating the signal (Figure 1.4):

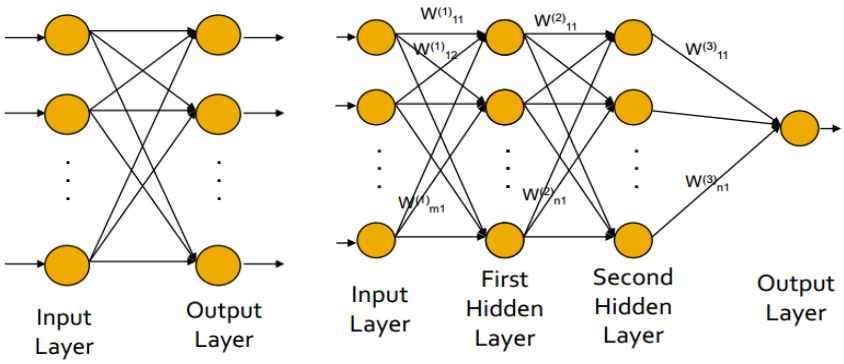

Figure 1.4: Example of neural network with single (left) and multiple (right) layer

The procedure that consists in estimating the parameters of neurons so that the whole network can perform a specific task is called *learning*: in supervised learning, the neural network output is compared with the "truth" and by a feedback process the network modifies the parameters to better approximate the desired outputs; instead, in unsupervised learning there isn't a feedback and the network finds itself the correlations between the data.

Extensive investigations of computerized image analysis for detection or diagnosis of abnormalities in a variety of 2D and 3D medical images have been conducted: most publications on CAD have been concerned with 3 organs, chest, breast, and colon, but other organs, such as brain, liver, and skeletal and vascular systems also have been subjected to CAD research [1],[28]-[36].

Chest radiography is the most commonly performed procedure in medical imaging; however, interpretation of chest radiographs is a difficult task because of the overlapping ribs and its low contrast sensitivity for subtle abnormalities, so the detection accuracy for lung nodules in chest radiographs could be significantly improved with the use of CAD [37]-[39].

The recommended annual screening mammography for women over 40 years of age results in a large volume of mammograms to be read by radiologists. Studies indicate that the false negative rate of mammography ranges from 10% to 30% because mammographic signs of breast cancer such as microcalcifications and masses can be very subtle and often obscured by dense breast tissue [28], [33]. This is the reason why computerized analysis systems for mammography usually are focused on the detection of either clustered microcalcifications or mass lesions [40]-[42].

Computed Tomography Colonography (CTC) is another important area of application of CAD. Colon cancer is the third leading cause of cancer deaths for men and women in the United States. Colon cancer screening involves detection of polyps, which can be the precursor of colon cancer, and cancerous growths on the walls of the large intestine. Interpretation of CTC is time consuming and difficult because the radiologist's sensitivity of polyp detection in CTC varies over a wide range, which was attributed to many factors such as the variability in CT scanning techniques, colon preparation methods, size of the polyps in the studied patient cohort, and the radiologists' experience with CTC. CAD may be a useful adjunct to CTC to reduce false negatives and reader variability. The current CTC CAD systems have sensitivity ranging from 80% to 100% at an FP rate of 2 to 15 per scan [43]-[45].

Recently, a new application of CAD systems is the diagnosis of autoimmune diseases based on research and identification of antinuclear autoantibodies (ANAs) through indirect immunofluorescence (IIF). However, it is a labor-intensive assay and highly dependent on the skills of the reader. Indeed IIF needs to be upgraded in order to overcome the following current major limitations of the method: the lack of resources and adequately trained personnel, the low level of standardization, the interobserver variability, the photobleaching effect.

The consequence of current debate on automation in ANAs test is that the ability to automatically determine the presence of autoantibodies in IIF would enable easier, faster and more reliable tests execution, faster result reporting, increase test repeatability, and lower costs [46]-[48]. For the standardization of a methodic as valid support in the diagnosis of the autoimmune diseases [49]-[51], computerized methods and software have been proposed for the support to the diagnosis.

1.2 Autoimmune Diseases

Autoimmune diseases are a family of more than 80 chronic, and often disabling, illnesses that develop when underlying defects in the immune system lead the body to attack its own organs, tissues, and cells. These disorders are fall into two general

groups: systemic autoimmune diseases (e.g. multiple sclerosis) and organ specific autoimmune diseases (e.g. diabetes) (Figure 1.5).

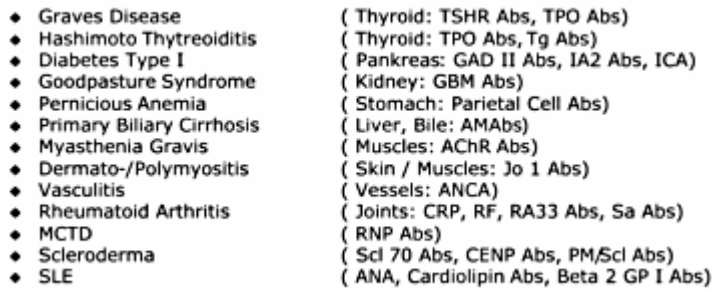

Figure 1.5: A short list of autoimmune diseases

While many of these diseases are rare, collectively they affect 14.7 to 23.5 million people only in USA [52], and – for reasons unknown – their prevalence is rising. Since cures are not yet available for most autoimmune diseases, patients face a lifetime of illness and treatment. They often endure debilitating symptoms, loss of organ function, reduce productivity at work, and high medical expenses. And, because most of these diseases disproportionately afflict women and are among the leading causes of death for young and middle-aged women, they impose a heavy burden on patients' families and on society.

The burden of a human disease should be counted not only in terms of money spent on health care for people directly affected, but as the total cost to society. It must take into account the number of individuals who are ill and the direct and indirect effects of the illness on patients, their families, their associates, and the public. Patient and family burden may include economic losses, altered or abandoned career or educational goals, and stress, suffering, and uncertainty. The first step in managing patients with any disorder is proper diagnosis.

Diagnosing autoimmune diseases can be particularly difficult, however, because these disorders can affect any organ or tissue in the body, and produce highly diverse clinical manifestations, depending on the site of autoimmune attack. Moreover, disease symptoms are often not apparent until the disease has reached a relatively advanced stage.

Diagnosis of an autoimmune disease typically begins with a careful health history, including assessment of possible occupational and environmental exposures. Many of the early symptoms of these disorders, such as fatigue, joint and muscle pain, fever, or weight change, are nonspecific. While these symptoms alone may not point to a particular autoimmune disease, when considered in retrospect they can help to pinpoint when the disease process began. Added diagnostic clues may be revealed through family history, as the presence of autoimmune disease in a patient's family further suggests that an autoimmune disease should be considered among the diagnostic possibilities. Similarly, a social and occupational history may identify exposures associated with a particular autoimmune disorder [52].

Laboratory's techniques able to point out and confirm diagnosis of autoimmune pathologies are based on research and identification of auto antibodies, revealed by the presence of specific antigen- antibody complexes. Particularly, identification of antinuclear antibodies (ANA) is an important part of clinical medicine and clinical immunology. ANA testing for the assessment of systemic and organ-specific autoimmune diseases has increased progressively since immunofluorescence techniques were first used to demonstrate antinuclear antibodies in 1957. ANA tests are amongst the most commonly performed antibody tests world-wide and the most frequently performed test in many clinical immunology laboratories [53].

Antinuclear antibody tests have their origin in the lupus erythematosus cell (L.E.cell) phenomenon. This was first demonstrated in patients with systemic lupus erythematosus (SLE) in 1948 by Hargraves, Richmond and Morton whilst working at the Mayo Clinic. The L.E. cell test became widely used but was rather insensitive and difficult to standardise. In 1950, Coons and Kaplan working in Boston, described the use of fluorescein-labelled antibodies for identifying tissue antigens. At that time Lee, Michael and Vural (1951) showed that the L.E. cell phenomenon was caused by a gamma globulin protein which was probably an antibody.

In 1957 Holborow, Weir and Johnson (Canadian Red Cross Memorial Hospital, Taplow, UK) used the fluorescent labelled antibody technique to demonstrate that the sera of L.E. cell positive patients contained antibodies that produced homogeneous nuclear fluorescence on human tissues. It was soon clear that different patterns

occurred and in 1961 Beck (National Institute for Medical Research, London) used rat liver sections to demonstrate homogeneous, speckled and nucleolar staining of nuclei in sera from patients with a variety of different rheumatic diseases [53].

In the early days of ANA testing, rodent tissue (stomach, liver and/or kidney) was commonly used as the substrate. Rodent tissue however had several drawbacks such as small cell size, a lack of dividing cells (mitotics) and poor antigen expression that made interpretation of ANA patterns difficult. In the 1980s, cultured cell lines were examined for utility as an ANA substrate and the human epithelial- like cell line HEp-2 gained popularity. HEp-2 cells are a highly sensitive substrate that provide qualitative information which can be used as the initial step for more specific identification and quantification of autoantibodies. HEp-2's advantages over rodent tissue are:

1. A more sensitive substrate that allows identification of many patterns.
2. Human origin ensures better specificity than animal tissues.
3. The nuclei are much larger so complex nuclear details can be seen.
4. The cell monolayer ensures that all nuclei are visible.
5. Cell division rates are higher so that antigens produced only in cell division are easily located e.g. centromere and mitotic spindle patterns.
6. Antigen distribution is uniform.

The diagnosis of autoimmune pathologies is based on research and identification of antinuclear autoantibodies (ANAs) through immunofluorescence. Immunofluorescence is a technique allowing the visualization of a specific protein or antigen in cells or tissue sections by binding a specific antibody chemically conjugated with a fluorescent dye such as fluorescein isothiocyanate (FITC). There are two major types of immunofluorescence staining methods: 1) direct immunofluorescence staining in which the primary antibody is labeled with fluorescence dye, and 2) indirect immunofluorescence staining in which a secondary antibody labeled with fluorochrome is used to recognize a primary antibody (Figure 1.6).

Immunofluorescence staining can be performed on cells fixed on slides and tissue sections.

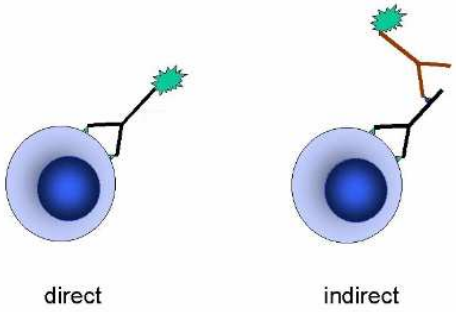

Figure 1.6: Direct and indirect immunofluorescence

Immunofluorescence stained samples are examined under a fluorescence microscope which emit infrared light (<750 nm): fluorescent marker absorbs the light and it re-emits with wavelength equal to ~ 700 nm (red light) or 530nm (green light) (Figure 1.7).

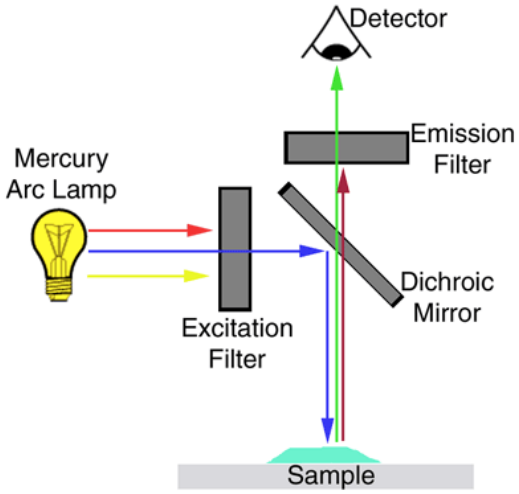

Figure 1.7: Fluorescence microscopy

The diagnosis is based on two parameters: the fluorescence intensity and the fluorescence pattern.

The fluorescence intensity is scored semi-quantitatively from 1+ to 4+ relative to the intensity of a negative and a positive control (4+), by following the guidelines established by the Centers for Disease Control and Prevention in Atlanta, Georgia (CDC) [54]:

- 4+ brilliant green (maximal fluorescence);
- 3+ less brilliant green fluorescence;
- 2+ defined pattern but dim fluorescence;
- 1+ very subdued fluorescence.

The pattern depends on the distribution of the antigen inside the nucleus: antibodies against antigens in different location give different patterns of fluorescence and therefore they allow the identification of the different diseases.

In the literature, staining patterns are classified into one of the following groups:

- homogeneous: diffuse staining of the interphase nuclei and staining of the chromatin of mitotic cells;
- speckled: a fine or coarse granular nuclear staining of the interphase cell nuclei;
- nucleolar: large coarse speckled staining within the nucleus, less than six in number per cell;
- cytoplasmic: fine fluorescent fibres running the length of the cell; it is frequently associated with other autoantibodies to give a mixed pattern;
- centromere: several discrete speckles distributed throughout the interphase nuclei and characteristically found in the condensed nuclear chromatin during mitosis as a bar of closely associated speckles.

Examples of the above defined patterns are shown in the Figure 1.8.

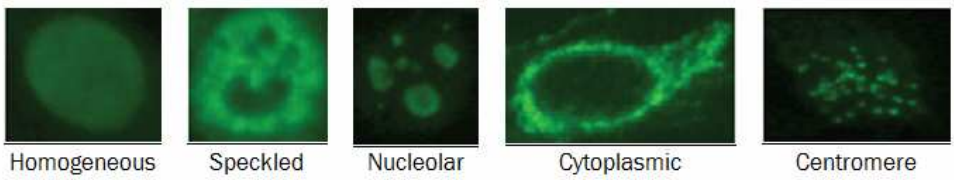

Figure 1.8: Examples of fluorescent patterns

Following the recent statement made by the American College of Rheumatology that the IIF technique should be considered as the standard screening method for the detection of ANA, the biomedical industry has proposed technological

solutions which significantly improve the automation of the procedure, not only in the preparation of substrates and slides, but also in microscope reading. This innovation is based on the principles of digitalization of fluoroscopic images and on the classification of patterns using standardized approaches (automated positive–negative screening and pattern interpretation). These systems are based on the use of automated microscopes, robotized slide trays, high-sensitivity video cameras, and software dedicated to acquisition and analysis of digital images [55]. The expected advantages of an automated IIF method are (a) the reduction in frequency of false negative and false positive results due to the standardization of measurement of fluorescence intensity; (b) the reduction of intra- and inter-laboratory variability; (c) improvement in the correlation of staining patterns with corresponding autoantibody reactivity; and (d) higher throughput in the laboratory workflow [55].

1.3 State of the art

Developing an automated procedure for diagnosis of autoimmune diseases, authors focus their attention on HEp-2 cell detection, on fluorescence intensity determination or on staining pattern classification. In the following paragraphs the state of the art related to these main topics will be presented.

1.3.1 State of the art on HEp-2 cell detection

With reference to HEp-2 cell detection, Chiang et al. [56] in 2010 proposed an efficient segmentation method for automatically detecting cells with fluorescence pattern in IIF imaging. The proposed method utilized the circle Hough transformation to separate connected cell in IIF images. The method evaluated 7614 cells with six distinct fluorescence patterns (including 620 diffuse patterns, 1077 peripheral patterns, 2251 coarse speckled patterns, 1509 fine speckled patterns, 852 discrete speckled patterns and 1305 nucleolar patterns) from 113 IIF images. Accuracy and sensitivity were used to estimate the performance of the proposed method. The results of

computer simulations revealed that the proposed method always identified cell outlines as were obtained by manual sketched with an accuracy of 88.77% and a sensitivity of 93.43%.

Huang et al. [57]-[57], proposed two method for automatically detecting outlines of fluorescence cells in IIF patterns: an adaptive edged-based segmentation method and a watershed segmentation method.

In the adaptive edged-based segmentation method [57], authors evaluated 2573 cells with six distinct fluorescence patterns (including 519 diffuse patterns, 482 peripheral patterns, 788 coarse speckled patterns, 634 fine speckled patterns, 64 discrete speckled patterns and 86 nucleolar patterns) from 45 images. In order to extract precise cells in an image, the proposed method comprised a simple classification procedure for IIF images to avoid over-segmentation. Firstly, the automatic thresholding algorithm was performed to convert an IIF image to binary version. Then the proposed method counted the number of connected region in the binary image. The information of the connected region was used as the input of the IIF image classifier. The proposed adaptive segmentation system obtained a stable and high accuracy; the proposed system clearly yielded cell outlines that are similarly to those manually sketched.

In watershed segmentation method [58], a two staged watershed transform automatically extracts outlines of cells in IIF images. In the first stage segmentation, the green channel from the original RGB image was utilized as input intensity to segment cells. After preprocessing, the proposed method employed the watershed transform to segment cell region. For reducing over-segmentation, the region merging procedure was utilized to merge the small connected regions. The region elimination procedure removed the segmented region with an unreasonable size. In the second stage segmentation, the method based on the concept of markers was utilized for controlling over-segmentation. The second stage module utilized the cyan component as input to avoid over-segmentation. The original RGB image was transformed to CMY (Cyan, Magenta, and Yellow channels) color space, the Otsu's algorithm was first performed to generate the marker for watershed segmentation. The similarity based watershed algorithm is performed herein to control over-segmentation in the

images. The paper evaluated 2305 autoantibody fluorescence patterns with manual sketched outlines (including 456 diffuse patterns, 417 peripheral patterns, 719 coarse speckled patterns, 55 fine speckled patterns, 517 discrete speckled patterns and 141 nucleolar patterns) from 44 IIF images. The performance measures, i.e. true-positive (TP), false-negative (FN), false-positive (FP) and sensitivity, were used to estimate the performance of the proposed system. The sensitivity was of 94.7%.

Percannella et al. [59] in 2012 proposed a new method for cells segmentation in HEp-2 images which adopts image reconstruction for a preliminary image segmentation and, then, employs a sort of classifier-controlled dilation for better determining the structure of the cells, where the classifier is trained using data of the image at hand. The authors used a public dataset of HEp-2 images, available at http://mivia.unisa.it/databases/db_database/biomedical/, which consists of 28 annotated IIF images. Images belong to two classes of fluorescence intensity, namely borderline and positive, and exhibit one of the main six staining patterns (homogenous, fine speckled, coarse speckled, centromere, nucleolare, cytoplasmic). The use of images with different fluorescence intensity and the low contrast of borderline samples as well as the staining pattern variability make the segmentation task more complex. To evaluate the performance of the proposed segmentation method, authors computed precision (Prec = TP/TP+FP), recall (Recall =TP/TP+FN) and f-index (f - index = 2·Prec·Recall/Prec+Recall) obtaining the values of60%, 43.8%, 50%, respectively.

1.3.2 State of the art on fluorescence intensity classification

With reference on fluorescence intensity classification, Soda and Iannello in 2006 and in 2009 proposed an ANN-based classifier [60] and a Multiple Expert System [61] classifier. In the first method, authors populated a database of 540 annotated IIF images; in order to label the data set samples and getting the ground truth for this specific application, they made use of two different physicians which independently diagnosed each sample. Each image of the data set was pre-elaborated in order to improve the contrast; then morphological filters, such as erosion and dilation have been applied to remove noise. Using Otsu’s algorithm, automatic thresholding was

performed to locate the cells. From these segmented images, they extracted a set of features, related to measures of fluorescent intensity, which are chosen considering the physician expertise. Also features of positive and negative controls have been considered. Authors investigated several classifiers, varying both the number of hidden layers and the number of neurons for layer, belonging to the family of Artificial Neural Network (ANNs) architectures: the Multi-Layer Perceptrons (MLPs) and the Radial Basis Network (RBF). All classifiers exhibited FP and FN rate approximately less than 1%; MLPs expert showed an overall error rate (FP plus FN) of 0.8%, whereas for the RBF such a percentage is 1.9%; RBF network exhibited a hit rate higher than MLPs expert (52.7% vs. 43.7%).

In the second paper, the recognition system is based on a multiple expert system (MES) paradigm and employs a classifier selection approach. Authors populated a database of 600 IIF images, revised by two physicians, which indicated three classes, named negative, intermediate and positive. The multiple expert system aggregates three different experts, each one specialized in recognizing one of three input classes (i.e., positive, negative, intermediate). Each expert is a nearest neighbour (NN) classifier. To combine the outputs of the classifiers, authors proposed two selection rules: a binary rule and a zero-reject selection rule. The former one is based on the binary combination of the output of single classifiers, whereas the latter rule is based on the evaluation of the reliability of each recognition act of the classifiers. These rules have been experimentally evaluated, exhibiting an error rate (FP plus FN) less than 0.9%.

1.3.3 State of the art on pattern recognition

With reference on pattern recognition, Soda in 2007 proposed a method based on a Multiple Expert System (MES) [62] in which the whole well staining pattern is computed on the strength of the recognition of its cells, testing two aggregation rules. To classify the well staining pattern into one of the basic groups (Homogeneous, Peripheral nuclear or Rim, Speckled, Nucleolar, No pattern) authors first segment the image to locate the cells; next, they classify the staining pattern of cells and, finally,

they classify the staining pattern of the whole well on the strength of the classification of its cells. They randomly select 28 images of fluorescent positive wells from a private database of IIF images. According to the classification approach, it is required to know not only the staining pattern of the whole well, but also the class of each cell inside them. In this respect, to locate the cells they use some morphological filters and global thresholding techniques.

The data set consists of 465 cells and the a priori probability of homogeneous, rim, speckled, nucleolar and artefact class (i.e. cell corrupted during the slide preparation process,) is 29.9%, 21.5%, 32.7%, 7.1% and 8.8%, respectively. To analyze the staining pattern they compute a set of features related to texture components, adopting both statistical and spectral features. The former measures are associated to properties of the first and the second order histogram, respectively (e.g. the moments up to the fourth order, the energy around the peak, the entropy). The spectral features are calculated by partitioning the spectrum of the Fourier Transform into angular and radial bins. The proposed MES aggregates five Nearest Neighbour (NN) classifiers, each devised to recognize one of the staining pattern classes. Every NN expert labels the input sample as belonging or not to its class, i.e. it has a binary output. Furthermore, each one uses a different features set. A selection module consisting of two selection rules computes the final output of the MES. With reference to staining pattern recognition of the whole well, by using the first selection rule correctly classifies the 70.5% of samples, misclassifies the 12.9% of wells and rejects the 16.6% of wells. Adopting the second rule, the hit rate is 62.2% , the miss rate is 8,3% and the reject rate is 29.5%.

Soda and Iannello proposed a Hybrid Multiple Expert System [63] in 2007 and a Multiple Expert System [64] in 2009.

In hybrid Multi-Expert Systems (MES), the MES is made up of L blocks with a binary output (i.e. 1 or 0) that indicates if the input sample belongs or not to the class on which it is specialized. Then, a selection module selects which block is most likely to be correct for any given input sample on the basis of two different selection rules: a Binary Selection rule and Reliability-based Selection rule. In order to populate a referring data set of fluorescent cells, authors randomly select 37 images of positive

wells from a private database. Two IIF specialists independently classify the pattern of each cell at a workstation monitor. Data set consists of 573 labelled cells. To analyze the staining pattern they compute a set of features related to texture components, adopting both statistical and spectral features. The former measures are associated to properties of the first and the second order histogram, respectively (e.g. the moments up to the fourth order, the energy around the peak, the entropy). The spectral features are calculated by partitioning the spectrum of the Fourier Transform into angular and radial bins. Furthermore features related to Wavelet Transform and Zernike Moments have been computed. The absolute performances of the Hybrid systems showed an hit rate of 60.8% for the Binary Selection rule and an hit rate of 75.9% for the Reliability-based Selection rule.

With the MES method, authors first segment the image to locate the cells and extract the features; second, they label the staining pattern of individual cells, and third, they classify the staining pattern of the whole well on the strength of the classification of its cells. The MES is based on the one-per-class paradigm, which assumes that the multiclass learning problem is reduced to several binary classification tasks. Given the number L of classes among which the input samples are distributed, the MES is composed of L modules, each one being an expert in the separation of one input class from the others. Their predictions are aggregated to a final decision on the basis of a certain rule (the aggregation module) that identifies the module that is the most likely to be correct for any input sample. Each module can be constituted either by a single classifier or by employing again a multiple experts scheme. In the latter case, the classifiers combination technique can be based on fusion, selection, or a mixture of them. In particular, to improve the recognition performance attainable by the L modules, we implement them with multiple binary classifiers combined by fusion rule, namely the weighted voting (WV). The data set consists of 573 labelled cells, from images of 37 IIF wells. Two specialists of IIF independently and blindly classify about 15 cells per well, one at a time, which have been chosen at random from those segmented. The system attained a hit rate equal to 97.3%.

Perner et al. [49] in 2002 presented results on the analysis and classification of cells using image analysis and data mining techniques. Starting from a knowledge-

acquisition process with a human operator, authors developed an automatic image analysis and a feature extraction algorithm for the objective measurement of image features. They used a dataset containing 53 images for each of the six class (homogeneous, homogeneous fine speckled, nuclear, fine speckled, fine speckled nuclear, centromere). A dataset containing 132 features was set up and given to data mining tool to find out the best set of features and to construct the structure of the classifier. The classifier is a decision tree induction program which allows one to learn a set of rules and basic features necessary for decision making in a diagnostic task. The classifier was evaluated by cross validation: the error rate of the decision tree based on calculated image features is 25%.

Sack et al. in 2003 proposed a computer assisted system for classification of interphase HEp-2 immunofluorescence patterns in autoimmune diagnostics [51]. They utilized a software package developed by P. Perner based on a novel image analysis and feature extraction algorithm. The samples are 1041, with six pattern (Homogeneous, Nucleolar, Speckled, Peripheral nuclear, Nuclear dot, Mitosis asssociated). The image as imported from the camera module was transformed into a grey level image by intensity without consideration of colours. Pictures were normalized and processed by automatic thresholding as well as morphological filters like dilation and erosion. Finally, cells were cut out from the image. Data describing various of these singular cells were calculated and stored in a data base. The generated data set was then subject to machine learning techniques to find out relevant features for a correct classification of autoantibodies. Finally, a learning algorithm selected from the data set the most promising features and constructed the structure of a classifier. The classifier was evaluated by crossvalidation method. Beside taking the patterns for the assisting computer system, human operators contributed to the knowledge acquisition process by teaching the system by their knowledge. Two essential procedures can be performed: discrimination between positive and negative sera, and pre-classification of main patterns. The evaluation of the system revealed that a multiparameteric mixture of different image information is necessary for a correct classification of the pre-defined groups of fluorescence patterns. The system reaches more than 83% of correct classification.

Recently, Iannello et al. [65] presented a method extending the panel of detectable HEp-2 staining patterns, introducing the centromere and cytoplasmic patterns, which do not show well-defined cell edges, and where a segmentation-based classification may fail. They applied a local approach which extracts SIFT descriptors and then classifies an image through the bag of visual words approach (BOVW). BOVW is inspired by the bag of words approach originally introduced in text classification, where a document is categorized by counting the most recurring words. While in text documents a vocabulary is already determined, in the visual domain it must be defined. For this purpose the set of ROIs extracted from multiple training images can be clustered in k groups in the feature space. Treating each cluster as a visual word, authors get a visual word vocabulary encoding the information contained in all local patterns. Then, a test image is represented by a feature vector counting each visual word contained in that image. This permitted to represent complex image contents without applying the segmentation procedure. They tested their approach on a dataset of 176 HEp-2 images with large variability in both fluorescence intensity and staining patterns. Their system correctly recognizes the 98.3% of samples, with a F-measure equal to 92.3%, 95.2% and 99.0%, for each class.

In 2009, Hsieh et al. [66] proposed a classification method utilizing learning vector quantization (LVQ) with eight textural features (Standard deviation, Uniformity/Entropy, Block variation of local correlation (BVLC) coefficients, Spatial grey-level dependence matrices, Grey-level difference matrix, Neighbourhood grey-tone difference matrix, Fractal dimension, Image coarse degrees) to identify the fluorescence pattern. Learning vector quantization (LVQ) is a prototype-based supervised classification algorithm and can be understood as a special case of an artificial neural network, more precisely, it applies a winner-take-all Hebbian learning-based approach. LVQ was invented by Kohonen. The network has two layers: a layer of input neurons, and a layer of output neurons. The network is given by prototypes W = (w(i),...,w(n)). It changes the weights of the network in order to classify the data correctly. For each data point, the prototype (neuron) that is closest to it is determined (called the winner neuron). The weights of the connections to this neuron are then adapted, i.e. made closer if it correctly classifies the data point or made less similar if

it incorrectly classifies it. An advantage of LVQ is that it creates prototypes that are easy to interpret for experts in classification applications. The study evaluated 1036 autoantibody fluorescence patterns from 44 IIF images that were divided into six pattern categories (including diffuse, peripheral, coarse speckled, fine speckled, discrete speckled and nucleolar patterns). The simulations showed that the proposed system has an average accuracy of 80.3%.

Rigon et al. [46] in 2011 presented a comprehensive system that supports the two sides of IIF tests classification. It is based on two systems: the first labels the fluorescence intensity, whereas the second recognizes the staining pattern of positive wells. For the fluorescence intensity classification they used the “multi expert/modulesystem”. To asses fluorescence intensity each expert is specialized on one of the following classes respectively: positive, negative or intermediate (weak positive). For achieving the final decision on the image all the expert decision need to be combined. To this purpose they proposed two different rules that provide the final classification on the basis of dichotomizers outputs. The first consists of a binary combination of the expert/module's outputs, referred to as Binary Selection (BS) (conservative selection rule). This rule rejects sample when none module indicates that the sample belongs to its class or when there is no agreement between modules. This approach does not require any reliability estimation. Alternatively, they proposed a strategy based on reliability estimation that chooses an output in any of the possible combinations of modules' output may be introduced, referred to as Reliability-based Selection (RbS). For the staining pattern classification they first segment the image to locate the cells; second, they classify the staining pattern of several cells and, third, they classify the staining pattern of the whole well on the strength of the classification of its cells. To test the system dedicated to classify the fluorescence intensity, they populated a dataset of 600 images obtained from sera screened for ANA by IIF on Hep-2 cells. To carry out the recognition of staining pattern, the cells data set consists of 573 labelled cells. The error rate has been evaluated according to eight-fold cross validation method: with reference to fluorescence intensity classification, using binary selection rule (BS) the hit rate is 87.4%, using the RbS rule the hit rate increases from

87% up to more than 94%. With reference to cells pattern classification, using BS the hit rate was 60.8%, using RbS rule the hit rate was 75.9%.

Bossuyt in 2013 [67] evaluated detection of antinuclear antibodies by G-Sight (Menarini), an automated system for image acquisition and interpretation of indirect immunofluorescence based tests. They evaluated the ability of the system to estimate the fluorescence intensity and to correctly classify fluorescence patterns. The positive/negative discrimination is evaluated while the system is focusing over cells. The sensitivity of the camera is regulated over the entire image in order to reach a cell target density. The system was trained over a collection of sera in order to discriminate a positive or negative sample by evaluation of the parameters that regulate the sensitivity of the camera acquisition. A probability measure of positivity (probability index) is calculated based on statistics of a set of training samples. This probability index is used to classify the sample in positive, negative or uncertain. The system performs intelligent pattern recognition (five patterns can be assigned: homogeneous, nucleolar, speckled, centromere and mitochondrial). The first step in the image processing algorithm is the use of morphological operators and threshold techniques to separate background from foreground. The segmentation of foreground is performed in order to evaluate single cells. In a second step, texture features are calculated that evaluate the intensity surface of the cells. Finally, a supervised learning classifier is used to classify patterns by using the descriptors. Automated antinuclear antibody analysis by G-Sight was performed on 268 consecutive samples submitted to the laboratory. G-Sight allows assigning 5 basic fluorescence patterns and G-Sight correctly assigned a homogeneous, speckled, and centromere pattern in 28 (68%), 24 (71%), and 5 (83%) of these samples, respectively.

Elbischger et al. [68] focused on the development and evaluation of image processing and classification algorithms for HEp-2 cell segmentation and cell type classification in order to better detect a suspicion diagnosis for autoimmune diseases. A medical doctor has manually classified a set of images in 17 different cell type classes coming from five nucleus patterns (Homogeneous (H), Speckled (S), Centromere (C), Nucleolar PmScl (P) and Scl-70 (Sc)) and from the distinction between cells in interphase (icells) and mitosis phase (m-cells) with their four sub-

phases (Prophase, Metaphase, Anaphase, Telophase). Nine features are calculated from the segmentation results and are used in the classification task: Area ratio, Variance, Perimeter ratio, 30th and 60th normalized percentiles and percentile range, Dent number, Auto-covariance percentage, Roundness. A Mahalanobis distance classifier is used for classification. The system is capable of distinguishing the 17 classes with 90.25% accuracy.

Foggia et al. [69] focused on mitotic cells presenting an heterogeneous set of features used to describe the peculiarities of this type of cells and then tested five classifiers, belonging to different classification paradigms. The approach has been evaluated on an annotated dataset consisting of 126 cells, 63 mitotic cells and 63 no mitotic cells. To represent the peculiarities of mitotic cells authors used morphological descriptors inspired by the peculiarities of cells at hand and texture measures, e.g. first and second order histograms, rectangle features and local binary pattern (LBPs). The first set of features is composed by morphological descriptors, which are based on the observation that mitotic cells may be fluorescent inside or outside the chromosomes mass We compute features that, on the one side, look for elliptic shape and, on the other side, analyse the fluorescence intensity inside the cells. The second set of features consists of texture measures related to statistical and spectral measures. The former have been extracted both from intensity histogram and from grey level co-occurrence matrix by means of computing their statistical moments, e.g. skewness, kurtosis, energy, entropy, to name a few. The latter have been computed from Fourier transform (FT), Wavelet transform and Zernike moments. LBPs assign to each pixel of the image a label obtained comparing it with its neighbourhood matrix. Authors tested popular classifiers: a Multi-Layer Perceptron, a Naïve Bayes, a kNN, a Support Vector Machine, and an AdaBoost, obtaining an accuracy of 82.37%, 80.16%, 86.51%, 81.09%, 85%, respectively.

Ersoy et al. [70] presented a feature extraction and classification scheme to classify the fluorescence staining patterns of HEp-2 cells in IIF images. They proposed a set of features that are sensitive to staining pattern variations among classes: Edge-based features which capture both gradient magnitude and orientation information, Local shape-based features incorporated through three measures obtained from the

Hessian matrix (Hessian matrix H describes the second order structure of local intensity variations around each point of the image), Texture information incorporated through LBP Local binary pattern (LBP) defined as a grey-scale invariant texture measure. They applied a multi-view ShareBoost algorithm to this set using each feature descriptor as a separate view. ShareBoost utilizes a single re-sampling distribution for all views that helps the classifier to exploit the interplay between subspaces and is robust to noisy labels. They used the data set reported in [69] and made available with the ground truth for the ICPR 2012 HEp-2 cell classification contest (http://mivia.unisa.it/hep2contest/index.shtml). The experimental results show an average of over 90 percent accuracy in classification of six HEp-2 cell types (centromere, coarse speckled, cytoplasmatic, fine speckled, homogeneous, nucleolar).

Petter Strandmark et al. [71] introduced a classification method for mitotic cells in IIF images. Each mitotic cell is classified into one out of six categories (centromere, coarse speckled, cytoplasmatic, fine speckled, homogeneous, nucleolar). They used the data set from the HEp-2 Cells Classification contest (http://mivia.unisa.it/hep2contest/index.shtml) of the ICPR 2012. The method is based on random forests that classifies an HEp-2 cell image into one of six classes. A random forest computes averages over several hundreds of small decision trees, each of which is trained on a subset of the features and the training examples. The set of features include Number of objects, Area, Area of the convex hull, Eccentricity, Euler number, Perimeter etc. They obtained an accuracy of 97.4%.

Kuan Li et al. [72] presented four image descriptors for HEp-2 cell staining patterns classification, including LBP, Gabor, DCT, and a global appearance statistical descriptor. Staining patterns are classified into one of the following six groups: homogeneous, fine speckled, coarse speckled, nucleolar, cytoplasmic and centromere. A multiclass boosting SVM algorithm is proposed to integrate these descriptors together: (1) within each boosting round, four multiclass posterior probability SVMs are trained corresponding to four descriptors, and then combined to an integrated classifier; (2) AdaBoost.M1 is modified to enhance the performance of the integrated classifiers. Experimental results over 721 images obtained from ICPR2012 contest (http://mivia.unisa.it/hep2contest). The results are 98.62% ±1.24% in positive samples,

95.85% ± 1.64% in intermediate samples, and 96.83% ± 1.46% in the total 721 images. It shows that proposed method achieves better performance than other SVM using single descriptor.

V. Snell et al. [73] introduced a combination of spectral analysis and multiscale digital filtering to extract the most discriminative variables from the cell images. They also applied multistage classification techniques to make optimal use of the limited labelled data set. The contest training data consists of 721 images of individual cell IIF patterns, each having an associated binary mask, and intensity label (positive or intermediate), and a ground-truth class label from one of 6 classes (homogeneous, fine speckled, coarse speckled, nucleolar, cytoplasmic and centromere). Overall error rate of 1.6% is achieved in recognition of 6 different cell patterns, which drops to 0.5% if only positive samples are considered.

Ilias Theodorakopoulos et al. [74] proposed a system for automatic classification of staining patterns on single-cell fluorescence images. Their method utilized morphological features extracted from a set of binary images derived via multi-level thresholding of fluorescence images. Furthermore, a modified version of Uniform Local Binary Patterns descriptor was incorporated in order to capture local textural information. The classification was performed using a non-linear SVM Classifier. The proposed method was evaluated using a publicly available dataset, released for the purposes of HEP-2 Cells classification competition at ICPR 2012, achieving up to 95.9% overall classification accuracy.

Di Cataldo et al. [75] proposed a technique that performs automated classification of the staining pattern. Their method combined textural feature extraction and a two-step feature selection scheme to select a limited number of image attributes that are best suited to the classification purpose and then recognizes the staining pattern by means of a Support Vector Machine module. Experiments on IIF images of HEP-2 Cells classification competition at ICPR 2012 showed that their method is able to identify staining patterns with average accuracy of about 87%.

Wafa Bel haj ali et al. [76] tested a learning algorithm on cellular images acquired for the analysis of pathologies. In order to evaluate the automatic classification performances, they tested their algorithm on the HEp- 2 Cells dataset of Foggia et al.

(CBMS 2010). Results showed classification precision larger than 96% on average. The same authors et al. [77] proposed a novel automated approach for the categorization of cells in fluorescence microscopy images. Their supervised classification method aimed at recognizing patterns of unlabeled cells based on an annotated dataset. First, the cell images needed to be indexed by encoding them in a feature space. For this purpose, they proposed tailored bio-inspired features relying on the distribution of contrast information. Then, a supervised learning algorithm was proposed for classifying the cells. They carried out experiments on cellular images related to the diagnosis of autoimmune diseases, testing the classification method on the HEp-2 Cells dataset of Foggia et al (CBMS 2010). Results showed classification precision larger than 96% on average.

Ghosh et al. [78] proposed feature extraction methods for automatic recognition of staining patterns of HEp-2 images (provided as a part of the ICPR 2012 HEp-2 Cells Classification Contest) to develop a Computer-Aided Diagnosis system and support the specialists' decision . They compared the performances of various individual and combined features and show that a combination of HOG(Histogram of Oriented Gradients), Texture and ROI(Region of Interest) features are best suited for our task achieving an overall accuracy of 91.13% using a Support Vector Machine as classifier.

Chapter 2

2. 1 The project A.I.D.A.

The increasing complexity in the management and analysis of biomedical data has created the urgency and the necessity of using information technologies which support the doctors in diagnosis. Information and Communication Technologies (ICTs) were successfully applied in medical imaging and, recently, to improve the diagnosis of the Autoimmune Disease. The introduction of modern approaches based on computer systems represents an economic and effective support for the diagnosis of autoimmune diseases. In this context is inserted the project **A.I.D.A**. (Auto-Immunité: Diagnostic Assisté par ordinateur), an international strategic project financed by EU in the ENPI cooperation program Italy-Tunis. The project will concern particularly the application of ICTs for the diagnosis of autoimmune diseases, reading by computer the images of test IIF.

The basic idea come up from the research group of Department of Physic and Chemistry of University of Palermo, which since many years develops activity in the field.

This project, with its strong character of cooperation Sicily-Tunisia in the scientific, cultural and sanitary context, joins well within the framework of the European politics of neighbourhood, with the objective of strengthen the integration between both banks of the Mediterranean Sea. The project answers the objective of the promotion of research and innovation, within the framework of a cooperation between

science parks, the support for the innovation in the processes of production and the distribution of information technologies.

Autoimmune diseases, as explained in paragraph 1.2, are multifactorial diseases, whose risk factors are genetic and environmental. From a population to another one the combinations of risk factors can vary, generating different epidemiological profiles. The interest in working with populations close on genetic plan and climatic conditions but different from the point of view of customs, food habits, cultural conditions, environmental factors, is obvious as far as we can envisage comparative analyses. So, the study of autoimmune diseases, in frontier regions as Sicily and Tunisia can certainly improve the knowledge of their pathogenesis and the spreading of involved genetic and environmental risks.

The project plans the installation, in hospitals of Sicily and Tunisia, of stations of reports for test IIF, with a innovative software developed at the University of Palermo.

The project involves researchers recruited among the best young people coming from the Universities in Palermo and Tunisi, placed side by side by an international team composed by physicists, computer engineers, physicians and biologists. The main actors directly concerned by this project are the scientists of the hospitals and university centers, the structures of management of the health as well as the technological poles. The contribution of this project in terms of improvement of the capacities of these actors concerns the acquisition of information and new methods as well as the help to the diagnostic decision.

The italian partners of the project are:

- University of Palermo
- Assessorato alla Sanità of Sicilian Region
- Provincia Regionale di Agrigento
- ASP-TP, U.O.C. of Clinical Pathology Hospital of Trapani

The tunisinian partners of the project are:

- Lab. of Genetic, Immunology of Human Pathologies, University of Tunis El Manar
- Institut Pasteur, Tunis
- Hospital Charles Nicolle, Tunis

- Ministry of Health, Tunis

Other hospital collaborate to the project (Hospital Buccheri La Ferla and Civic Hospital in Palermo, ASP in Agrigento and Hospital Ariana of Tunisi); to the project the Sidi Thabet Technological Pole of Tunisi and the Department of the Productive Activities of Sicilian Region also participate.

The project has as objective the improvement of the diagnosis of autoimmune diseases by IIF, thanks to the use of a computer system, developed by the spinoff CyclopusCAD of the University of Palermo, for acquisition of images, implementation of a digital database and processing of data by the installation, in the hospitals of Sicily and Tunis, of stations of report for the tests IIF. The computer-aided acquisition of the images of IIF interpreted by the clinicians will allow to generate a quantity of data accompanied with a collection of additional information through questionnaires. The Italian team, with its experience in medical imaging, will take care of the technical support for the acquisition and the management of this database.

The development and the validation of a software of reading of images of IIF adapted to the diagnosis of autoimmune diseases using the systems of artificial intelligence and a wide library of images acquired in a digital format, constitute a rather innovative approach, because there is no available exhaustive digital IIF database for the scientific community and the computer systems for the help to the tests IIF, at present available, are rare and in phase of development. While, the need in this type of software is real because the interpretation of the IIF is subjective and requires a double reader. Furthermore, this type of software is adaptable to the distance teaching and to the auto-learning.

2.2 Database of A.I.D.A. project

The database inherent to the project includes any cards of the patients (data and images) collected from the various tests of laboratory (ANA, AMA, ASMA, ANCA, APCA, EMA, etc.) with the consequent use of the various types of substrata (HEp-2

and tissues). For the purposes of this thesis only the data concerning the determination of the ANA tests have been used, by using as substratum the epithelial cells of human laryngeal carcinoma (HEp-2, American Type Culture Collection CCL 23), in which the expression and the integrity of the clinically significant antigens will be guaranteed (see Appendix A).

Fluoroscopic images have been acquired for all the persons included in the survey to whom it is suspected the presence of an autoimmune disease and for all the persons in the centers associated to the project. The database will contain all clinical informations about the patient.

To prepare the sample the following procedure has been applied:

1. In every session (in the first blade) a positive control and a negative control have been inserted;
2. Dilution of the sample 1:80 in PBS 0,01M, pH 7,2;
3. Incubation of sample diluted (25-30 µL) and the controls (25-30 µL) with the substrate of HEp-2 cells for 30’ at room temperature in a wet room;
4. Three washes of 5' with PBS;
5. Incubation with the conjugated anti-IgG FITC (25-30 µL) for 30’ at room temperature in a wet room;
6. Three washes of 5' with PBS;
7. Assembly of blades in the glycerol in 10 % in PBS with a small strip.

The reading of fluorescence microscope has been made with a magnification of 40X. The regions of interest of every fluorescent pattern have been acquired by a CCD camera with a 1280x960 pixels resolution in TIFF or JPEG format. During the acquisition of images, areas full of HEp-2 cells occupied the central region of the image. For every well (except CN and CP) three different images to the purpose of a “double reading” have been acquired.

The fluorescence intensity, as already indicated in paragraph 1.2, is scored semi-quantitatively from 0 to 4+ according to the intensity of a negative (0) and a positive control (4+), following the guidelines established by the Centers for Disease Control and Prevention in Atlanta, Georgia (CDC) [54]:

4+: brilliant green (maximal fluorescence);

3+: less brilliant green fluorescence;

2+: defined pattern but dim fluorescence;

1+: very subdued fluorescence.

0: negative

At this moment, the identified patterns have been classified according to the Table 2.1:

Table 2.1: List of images and patterns of AIDA database

PATTERN	NUMBER OF IMAGES
Centromere	51
Coarse Speckled	74
Fine Speckled:	111
Nuclear Homogeneous	308
Few Nuclear Dots	19
Nucleolar Clumpy	32
Nucleolar Homogeneous	40
Nucleolar Speckled	3

2.3 The MIVIA public database

The http://mivia.unisa.it website offers a database of Indirect ImmunoFluorescence (IIF) images. It is the outcome of a research project jointly conducted by the Mivia Lab of the University of Salerno and the University Campus Biomedico of Rome, with the financial support of "Regione Campania" within the project "Classification of Immunofluorescence Images for the Diagnosis of Autoimmune Diseases". In this website there is an annotated database of IIF images, acquired using slides of HEp-2 substrate at the fixed dilution of 1:80, as recommended by the guidelines.

IIF slides are examined at the fluorescence microscope, and their diagnosis requires both the estimation of fluorescence intensity and the description of staining pattern. The former is scored semi-quantitatively with respect to both positive and negative controls contained in each slide and the sample fluorescence intensity is divided into three classes, named negative, intermediate and positive. The latter suggests the localization of reactive nuclear antigens and may help clinicians in differential diagnosis of six pattern (homogeneous, fine speckled, coarse speckled, nucleolar, cytoplasmatic, centromere).

Specialists took HEp-2 images with an acquisition unit consisting of the fluorescence microscope (40-fold magnification) coupled with a 50W mercury vapour lamp and with a digital camera. The camera has a CCD with squared pixel of equal side to 6.45 µm. The images have a resolution of 1388×1038 pixels, a colour depth of 24 bits and they are stored in bitmap format. Specialists manually segment and annotate each cell at a workstation monitor since at the fluorescence microscope is not possible to observe one cell at a time, and report data on fluorescence intensity (according to the three classes reported above), pattern (according to the six classes reported above) and mitosis phase. Firstly, a biomedical engineer segmented the cells by the use of a tablet PC. Subsequently, each image was reviewed and annotated by a medical doctors specialized in immunology.

For each image the database provided a description file containing:

- Image's pattern and intensity;

- Objects seed points;
- Objects class: cell, mitotic cell, artefact (due to slides preparation process);
- Objects pattern (if is a cell): homogeneous, fine speckled, coarse speckled, nucleolar, cytoplasmatic and centromere.

The composition of the database is described in Table 2.2.

Table 2.2: List of images of public database MIVIA

PATTERN	**NUMBER OF IMAGES**
Centromere	6
Homogeneous	5
Fine Speckled	4
Coarse Speckled	5
Nucleolar	4
Cytoplasmatic	4

2.4 Characteristics of proposed method

The purpose of the proposed method is to allow the recognition of centromere patterns. The method is based on the grouping of centromeres present in the cells through the application of the K-means clustering algorithm.

The first step of the method is the reading of the image: images coming from the fluorescence microscope and acquired by a CCD camera in TIFF or JPEG format are RGB images with a preponderance of Red or Green component in accordance with the wavelength of the light re-emitted by the fluorescent marker. The images present in AIDA database and in MIVIA database have a preponderance of Green component.

An advantage of the proposed method is its application both to images with a low fluorescence intensity and to images with high fluorescence intensity. It is interesting to show the difference in spatial distribution of coloured components for an image

with low fluorescence intensity and an image with an high fluorescence intensity, both belonging to the AIDA database. An example of an image with low fluorescence intensity is showed in Figure 2.1.

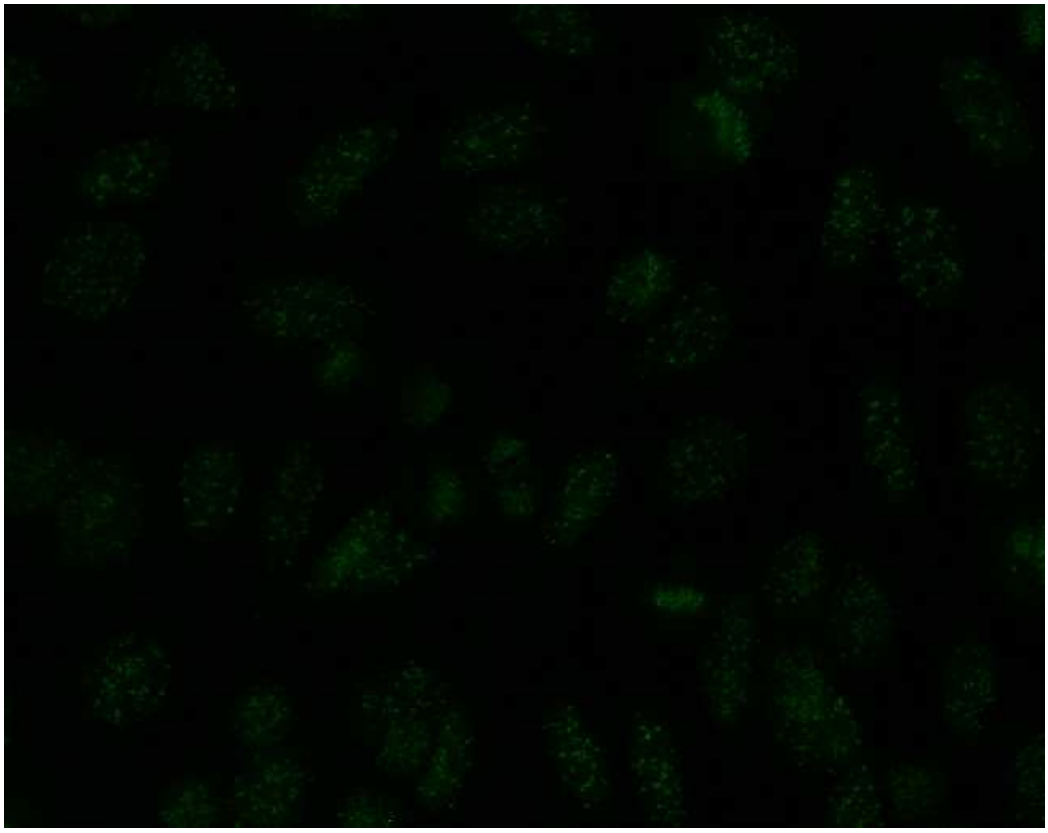

Figure 2.1: Example of an image with low fluorescence intensity

The Figure 2.2 shows the spatial distribution of the three component for the image in Figure 2.1.

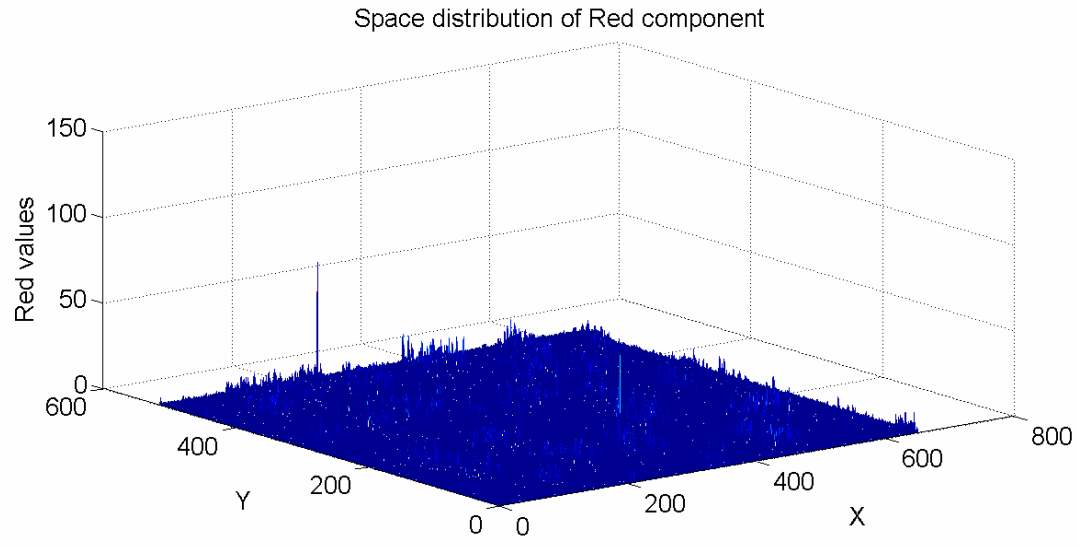

A

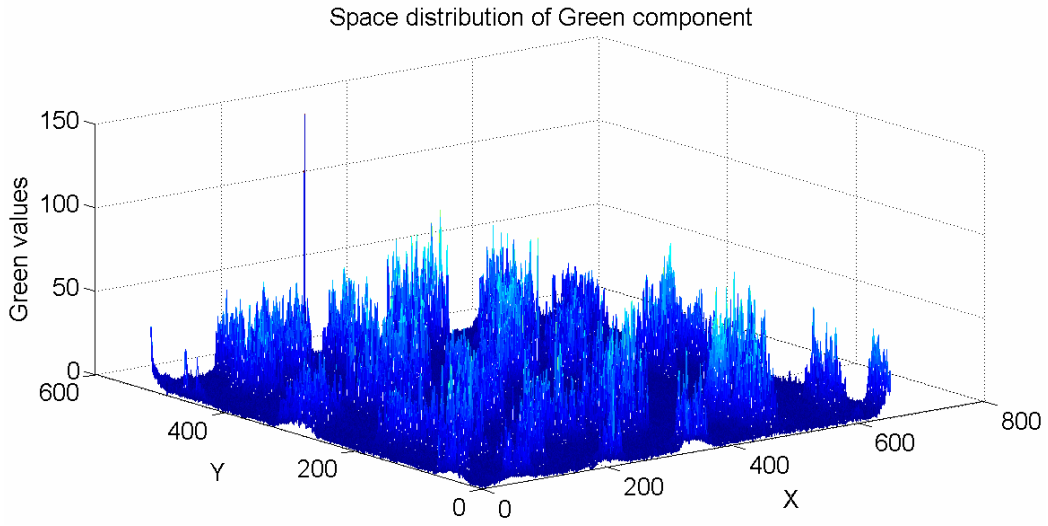

B

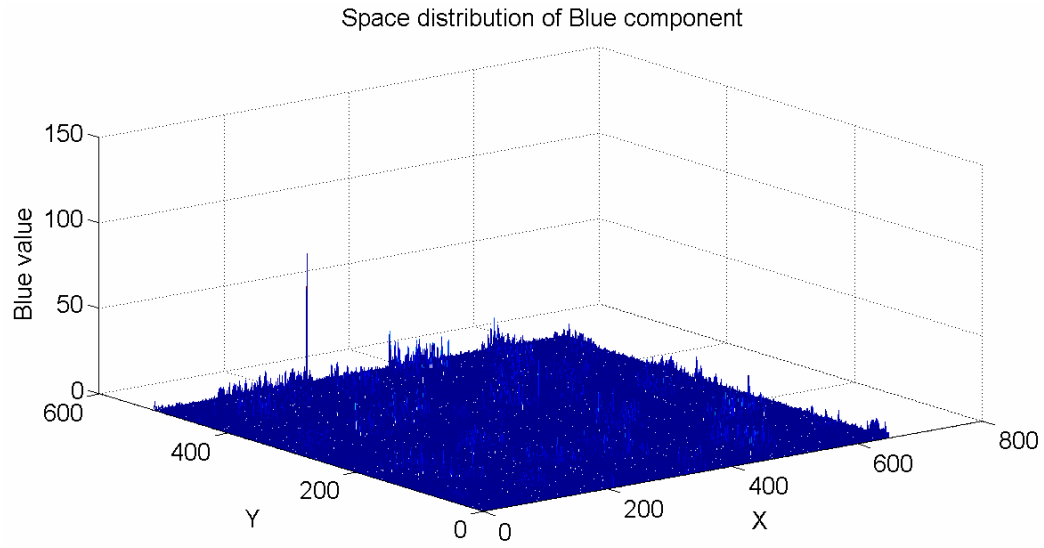

C

Figure 2.2: Spatial distribution of coloured components for a low fluorescence image: A) Red; B) Green; C) Blue

An example of an image with high fluorescence intensity is showed, instead, in Figure 2.3, and the Figure 2.4 shows the spatial distribution of the three coloured components.

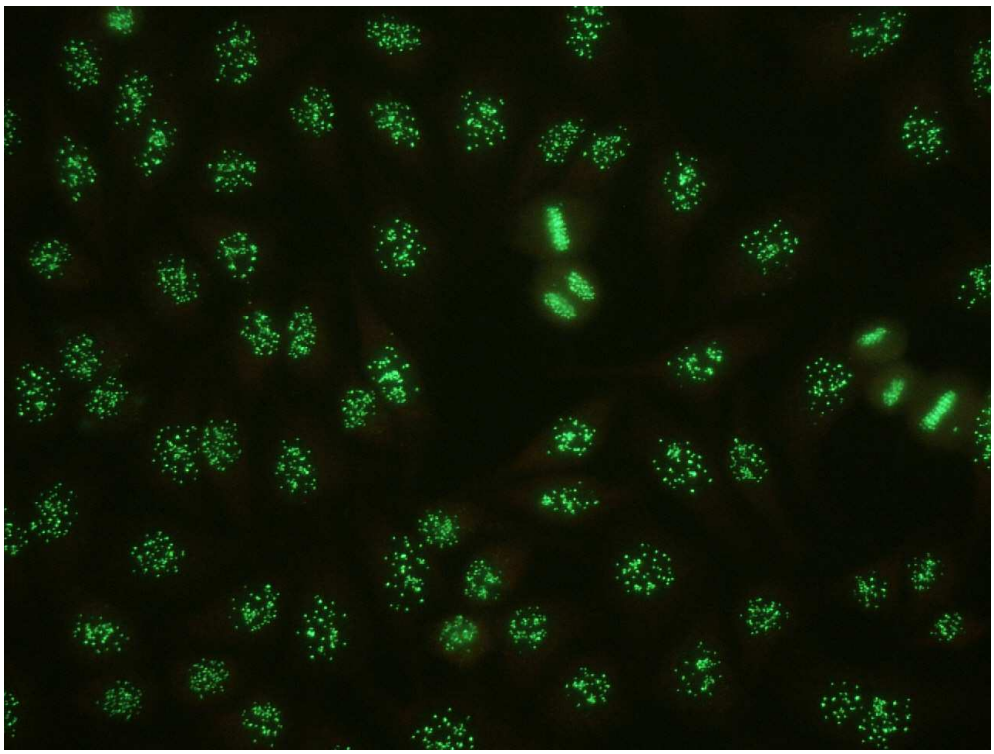

Figure 2.3: Example of an image with high fluorescence intensity

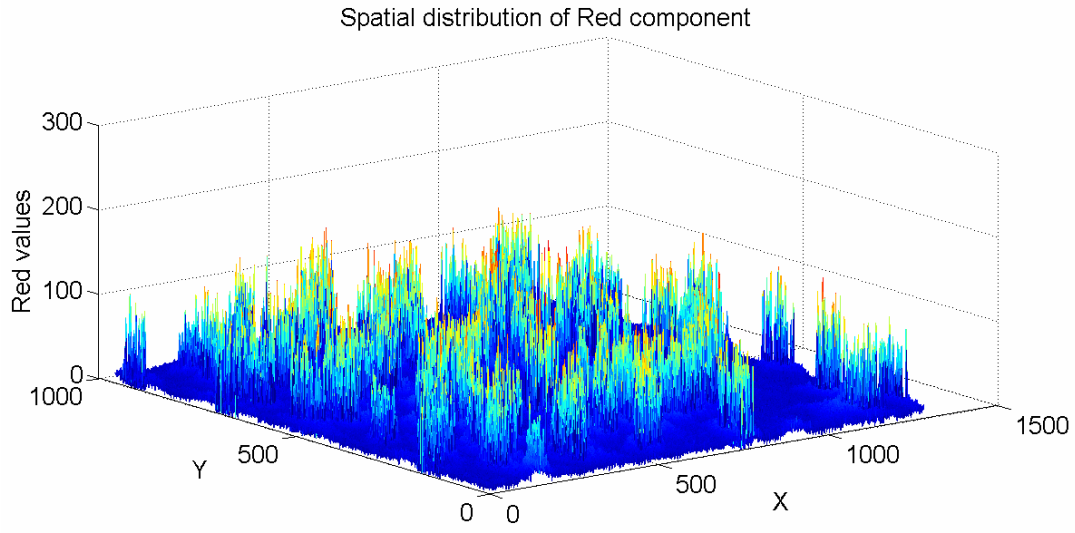

A

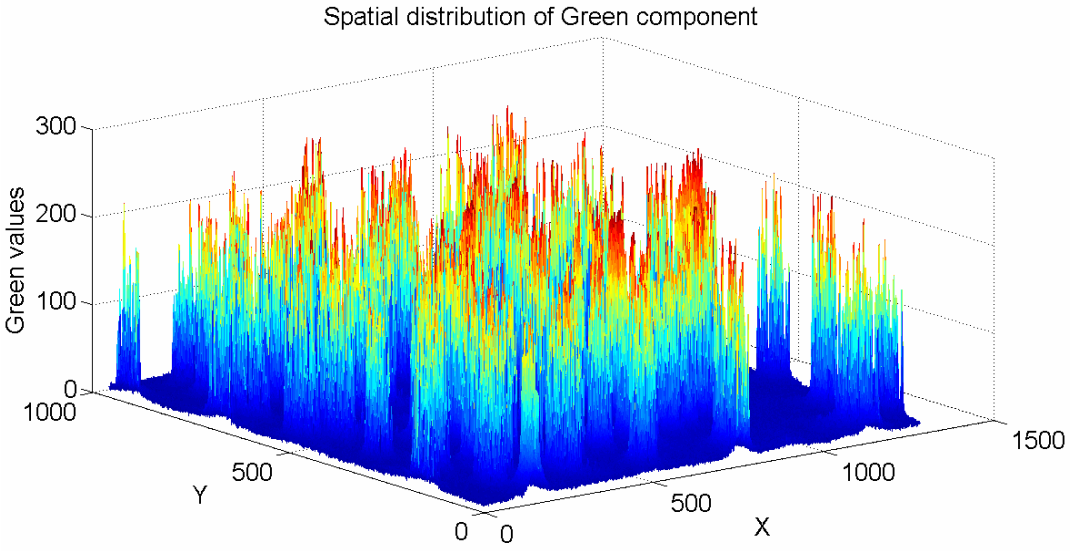

B

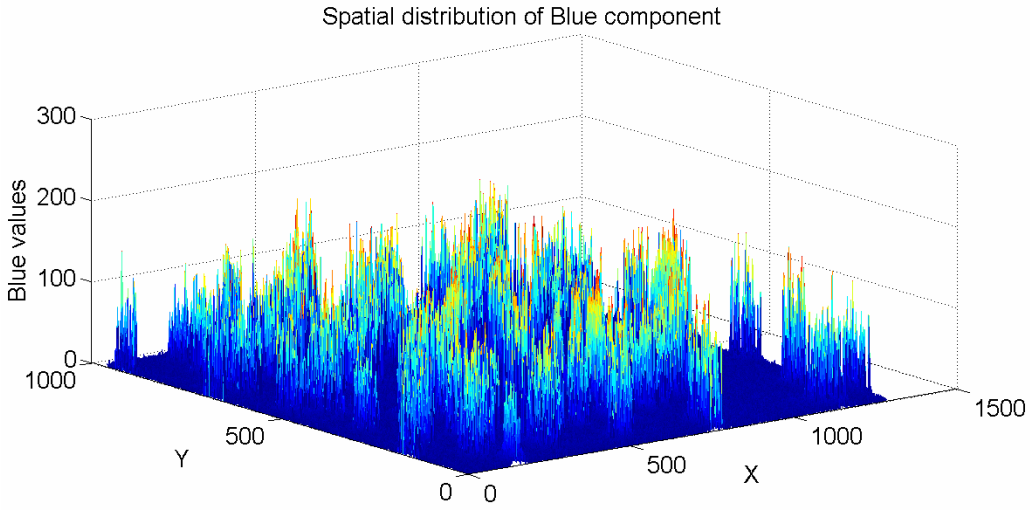

C

Figure 2.4: Spatial distribution of coloured component for an high fluorescence image: A) Red; B) Green; C) Blue

The observation of the spatial distribution of the three components of the RGB images confirmed us that the information about the fluorescence intensity is mainly contained in the Green component, so we focalize ourselves on this component only by converting the RGB images in grey images without loss of information.

The second step of the method is the preprocessing of the image which allows to automatically obtain the number of the cells and the coordinates of their centroids; as will be explain in Chapter 3, this operation is necessary to obtain the seeds for the K-means algorithm.

The first operation executed in the preprocessing phase is the contrast adjustment of images: starting from an image like that in Figure 2.5a) which is converted in a grey image, a method which implements a technique called *contrast-limited adaptive histogram equalization* (CLAHE) is used. CLAHE operates on small regions in the image, called *tiles*, rather than on the entire image. Each tile's contrast is enhanced, the neighbouring tiles are then combined using bilinear interpolation to eliminate artificially induced boundaries. The contrast, especially in homogeneous areas, can be limited to avoid amplifying any noise that might be present in the image.

After this operation, assuming the bright objects are the centromeres, it is possible to identify groups of pixels that are significantly higher than their immediate surrounding (Figure 2.5b).

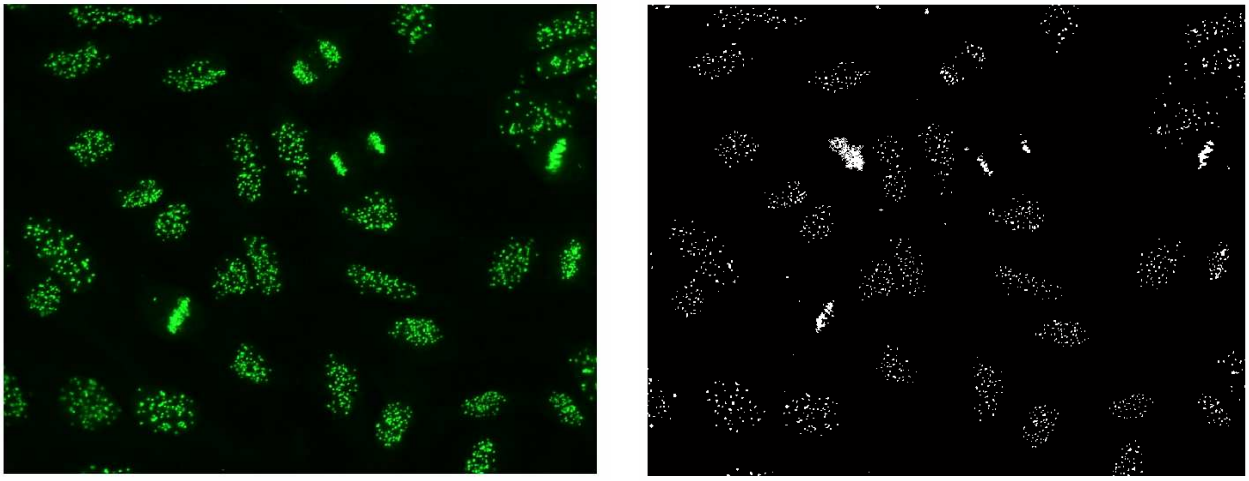

a) **b)**

Figure 2.5: a)Example of a centromere image; b) Image after contrast adjustment with CLAHE

To find the centroids of cells, morphological operations (see Appendix B) like *dilate* and *holes filling* are applied allowing objects to expand, connecting disjoint objects and filling in small holes and then, according to the literature, cells on board of slides are removed, because they can be artefacts or damaged. Finally, regions smaller than an Area threshold (fixed during the tuning phase which will be described in Chapter 3) are removed also, to obtain an image like that shown in Figure 2.6.

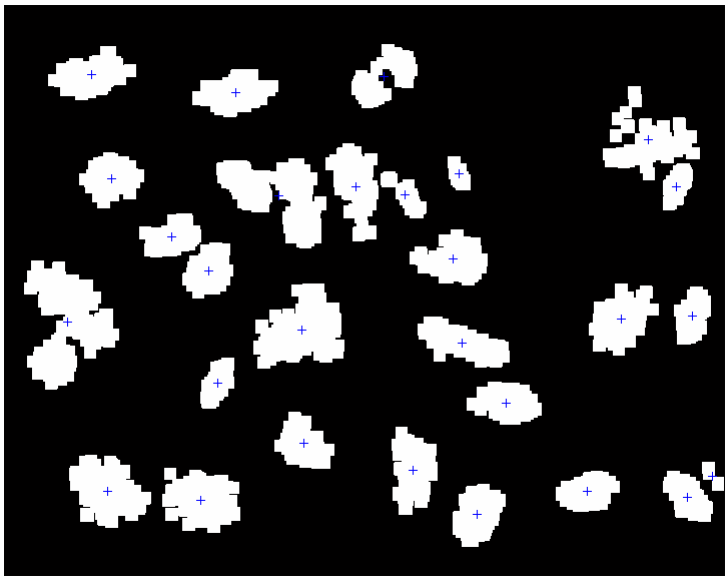

Figure 2.6: Centromere image after *dilation* and *holes filling* operation, with centroids

After this phase of preprocessing, it is possible to determine the coordinates of the centromeres belonging to the useful cells of the image and apply on them the K-means algorithm, which will be described in the next paragraph.

The application of the K-means has as result the number of elements belonging to the clusters and their relative centers: among all the clusters, only those containing the correct number of centromeres will be selected.

To avoid clusters too large compared to a real cell, another selection on clusters will be made based on the dimension of a cell, valued as the length of the Major Axis of an equivalent ellipse, which is another parameter determined during the tuning phase of the algorithm.

The final step of the method is the counting of the remaining clusters: if the number of clusters, i.e. the cells, is equal or great than a threshold called CUT, the image is classified as centromere.

As already explained, the tuning phase of the algorithm for the parameter Area, Major Axis and CUT will be described in details in Chapter 3.

The steps of the algorithm just described are shown briefly in the flow-chart in Figure 2.7.

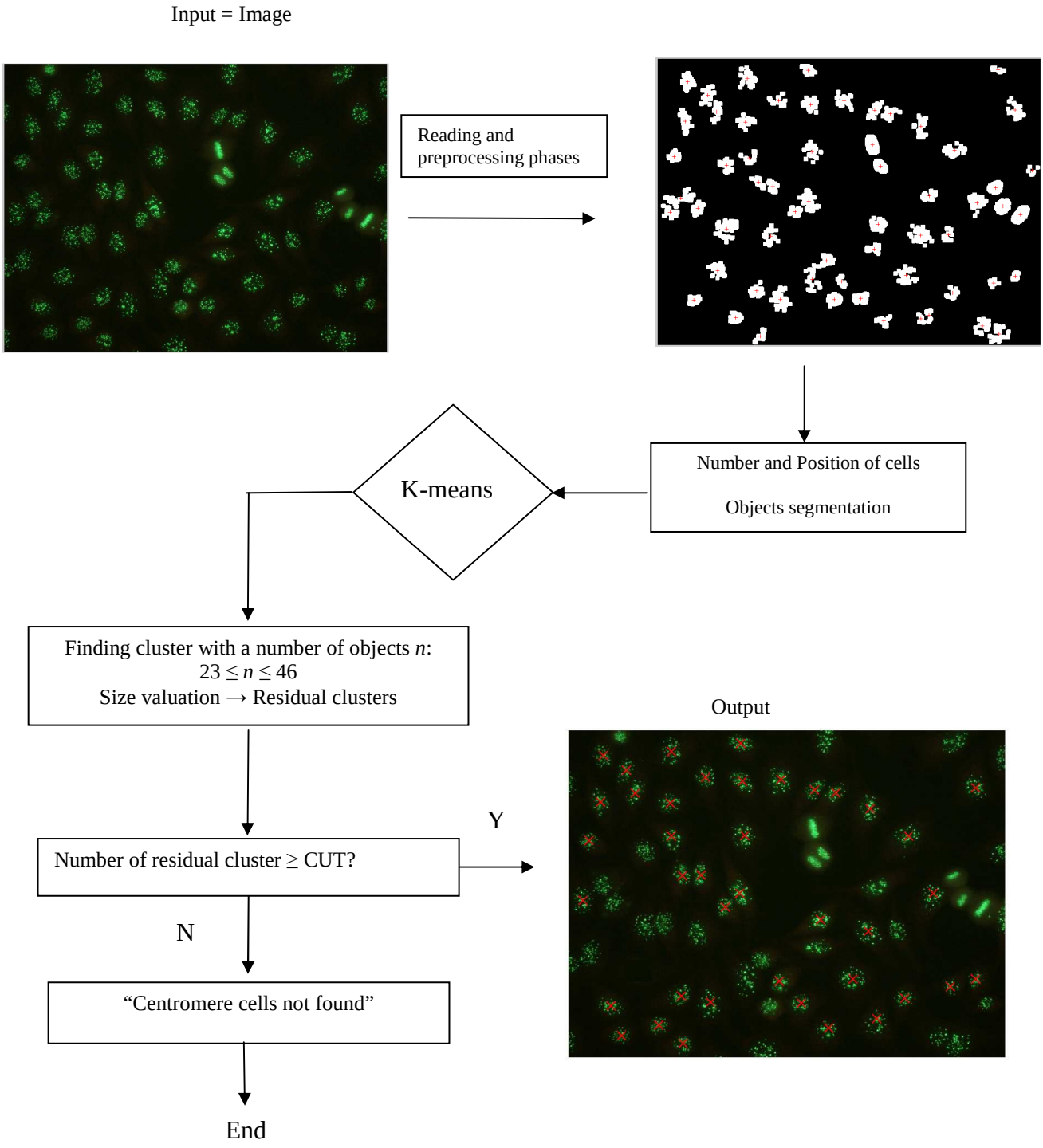

Figure 2.7: Flow-chart of proposed method

2.5 Clustering algorithms

Since an important part of the proposed method is based on a clustering algorithm, in this paragraph will be presented the general characteristics of these algorithms and of K- means in particular.

Generally, clustering is a classification imposed to a set of objects based on their characteristics [79]. There are many field of application of cluster analysis: biology, psychology, archaeology, marketing. In computer science and engineering, cluster analysis is used in pattern recognition and image processing, in unsupervised learning, vocal recognition, images segmentation.

As example, suppose we want to cluster four stars (Figure 2.8):

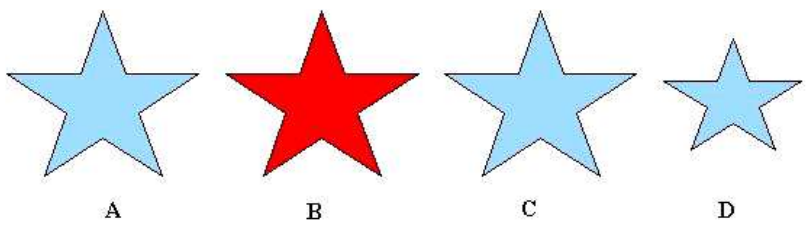

Figure 2.8 Example of objects to cluster

Stars A, B, C have same size, stars A, C, D have same colour, stars A and C have same size and colour. Size and colour are two characteristic (features) of objects "star" which can be measured and depicted as coordinates in a feature space. The relationship between objects or their features may be represented by ***similarity***, which has values in the interval [-1,1] or, if it is normalize, in the interval [0,1]. Similarity s_{ij} between feature *i* and feature *j* can be measured in many ways, depending from measure scales or data. Complementary to similarity is ***dissimilarity*** d_{ij} which measures the differences between objects based on their features. The relationship between similarity and dissimilarity is:

$$s_{ij} = 1 - d_{ij} \qquad (2.5.1)$$

Thinking to the objects as points in a *d*-dimensional metric space in which every dimension is a feature, it is possible to depict the relationship between objects as a pattern matrix (*n* objects with *p* features) or a proximity matrix, which contains the information on similarity or dissimilarity (Figure 2.9).

$$\begin{bmatrix} x_{11} & \cdots & x_{1f} & \cdots & x_{1p} \\ \cdots & \cdots & \cdots & \cdots & \cdots \\ x_{i1} & \cdots & x_{if} & \cdots & x_{ip} \\ \cdots & \cdots & \cdots & \cdots & \cdots \\ x_{n1} & \cdots & x_{nf} & \cdots & x_{np} \end{bmatrix} \quad \begin{bmatrix} 0 & & & & \\ d(2,1) & 0 & & & \\ d(3,1) & d(3,2) & 0 & & \\ \vdots & \vdots & \vdots & & \\ d(n,1) & d(n,2) & \cdots & \cdots & 0 \end{bmatrix}$$

a) b)

Figure 2.9 a) Pattern matrix (n objects with p features); b) Proximity matrix (similarity or dissimilarity)

Measuring similarity or dissimilarity of objects depends from the variables that characterize the objects: there are objects characterized by binary variables (Yes and No, True and False, Positive and Negative, etc…), nominal variables (Male and Female), ordinal variables (first, second, third, etc…), quantitative variables (cost, time, weight, etc...). Usually, dissimilarity is easier to measure than similarity because we can think to dissimilarity as "distance" in the multidimensional features space, so it is possible to calculate dissimilarity as Euclidean distance:

$$d_{ij} = \sqrt{\sum_{k=1}^{n} \left(x_{ik} - x_{jk} \right)^2} \qquad (2.5.2)$$

Clustering methods belong to two great groups: hierarchical and partitional methods. Hierarchical clustering uses only proximity matrix (Figure 2.9a), instead partitional clustering uses pattern matrix (Figure 2.9b). These classes will be described briefly in the next paragraphs.

2.5.1 Hierarchical clustering

A hierarchical clustering is a sequence of partition in which each partition is nested into the next partition in the sequence. The result of a hierarchical cluster is

depicted by a *dendrogram*, which allows to visualize how many objects were joined or separated during the process (Figure 2.10)

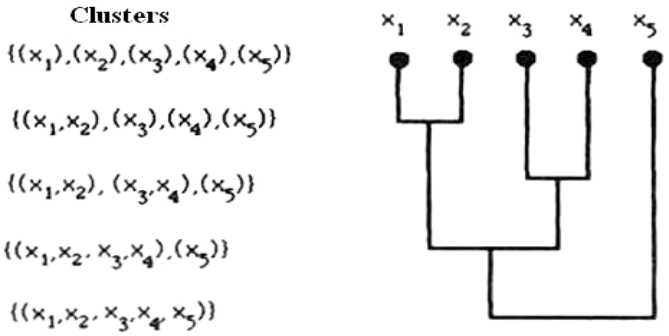

Figure 2.10 Example of a dendrogram

Partition with r clusters can be used to create a partition with r-1 clusters (agglomerative clustering) or with r+1 clusters (divisive clustering). Union or separation between clusters is made considering the distance, in features space, between clusters. The process stops when it is found the desired number of clusters or a limit on clusters diameter.

2.5.2 Partitional clustering

The non-hierarchical clustering methods are called partitional clustering. They generate a single partition of the data trying to reproduce the natural groups present in the data. The problem of this kind of clustering algorithm is to find the correct partition of the data so that objects belonging to the same cluster are more similar between them than to object belonging to other clusters.

Partitional algorithms are applied in ROI extraction process [80] ─ [83] or in image segmentation [84].

K-means algorithm is an example of partitional clustering [85]: starting with a set of n object x_j, to cluster in c groups G_i, the algorithm selects randomly c objects as

initial seeds and assigns the objects x_j to the cluster i if it is closer to the cluster centroid c_i than to other centroids; then, new centers of clusters are calculated according the equation 2.5.3

$$c_i = \frac{1}{G_i} \sum_{j=1}^{n} x_j \qquad (2.5.3)$$

The objects are assigned again and the process is repeated iteratively until a minimum of an objective function based on Euclidean distance between the object and the cluster centroids is reached (Figure 2.11).

Performances of K-means algorithm depend on initial choice of centroids, and the algorithm requires to know *a priori* the number of partition to find. Indeed, the K-means algorithm has good performances with sferical clusters, for this reason we chosen it to use in our application.

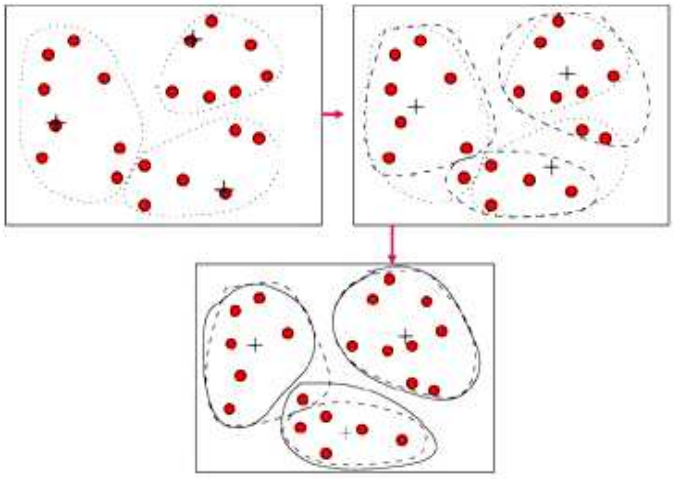

Figure 2.11: Example of evolution of K-means algorithm

2.6 Figures of merit

Suspecting a disease, a doctor generally can make one or more hypotheses based on the anamnesis and the objective examination. Such hypotheses are submitted to

verification through investigation-test, but such verifications are hindered by an intrinsic percentage of error in every test used; in fact, patients submitted to test A for the suspect of disease X can be *a posteriori*:

- **true positive** (TP): the test is positive and there is illness;
- **true negative** (TN): the test is negative and there isn't illness;
- **false positive** (FP): the test is positive but there isn't illness;
- **false negative** (FN): the test is negative but there is illness;

It is possible to define the ***Sensibility*** as the ability of the test to identify the presence of the illness:

$$\text{Sensibility} = \frac{TP}{TP+FN} \qquad (2.6.1)$$

Sensibility and FP define the reliability of the test, quantifying the tendency to result positive in the sick subjects and negative in the healthy subjects respectively [86].

In our case, to test the proposed algorithm we defined the following figures of merit:

$$\text{Sensibility\_images } \varepsilon = \frac{\text{number of images recognized centromere}}{\text{total of centromere images}}$$

$$\text{Sensibility\_cells } \eta = \frac{\text{number of cells recognized centromere}}{\text{total of cells}}$$

FP_{images} = number of images recognized centromeres (when the image is not centromere)

FP_{cells} = number of cells recognized centromeres (when the image is not centromere)

$$\text{Accuracy} = \frac{TP + TN}{TP + TN + FP + FN}$$

Chapter 3

3.1 Preliminary tests

The first step of the research activity was a preliminary testing of the proposed method on images coming from IIF tests on HEp-2 cells used to research and identification of antinuclear autoantibodies (ANA), and its validation based on the figures of merit defined in the paragraph 2.6.

The method was applied on centromere pattern, characterized by several discrete speckles (between 23 and 46) distributed throughout the interphase nuclei and characteristically found in the condensed nuclear chromatin during mitosis as a bar of closely associated speckles.

The database used for the preliminary testing was composed of the following patterns:

Table 3. 1 Database used for preliminary testing

Pattern	Nr. of images
Centromere	10
Nucleolar	18
Other	5

Because of the limited number of images used for the preliminary test, the error bars were really elevated (~ 3/10), so they have not been represented in the following graphics.

The algorithm classifies an image as centromere if it find almost *n* centromere cells, with *n* major than a threshold defined CUT The value of the CUT was variable in the interval [2, 10].

To test the performance of the proposed algorithm, the first figure of merit valued was the Sensibility_images, defined as:

$$\text{Sensibility\_images } \varepsilon = \frac{\text{number of images recognized centromere}}{\text{total of centromere images}}$$

The Figure 3.1 shows the Sensibility_images ε versus the CUT: as showed in the graphic, the algorithm had a constant value of Sensibility of 10/10 until the CUT = 6 and a constant value of Sensibility of 9/10 from CUT = 7 until the CUT = 10.

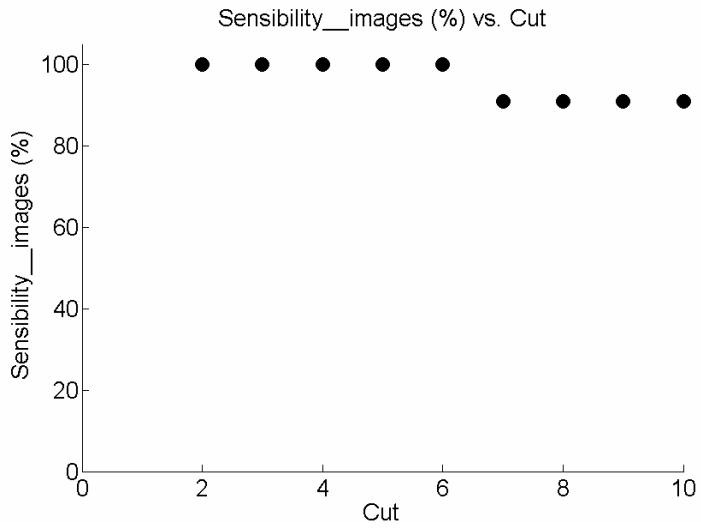

Figure 3.1: Graphic of Sensibility_images vs Cut

Another figure of merit valued was the Sensibility_cells defined as:

$$\text{Sensibility\_cells } \eta = \frac{\text{number of cells recognized centromere}}{\text{total of cells}}$$

The Sensibility_cells η was evaluated by repeatedly applying the algorithm on each centromere image: in Figure 3.2 is showed as example the graphic of η obtained for one of the centromere images.

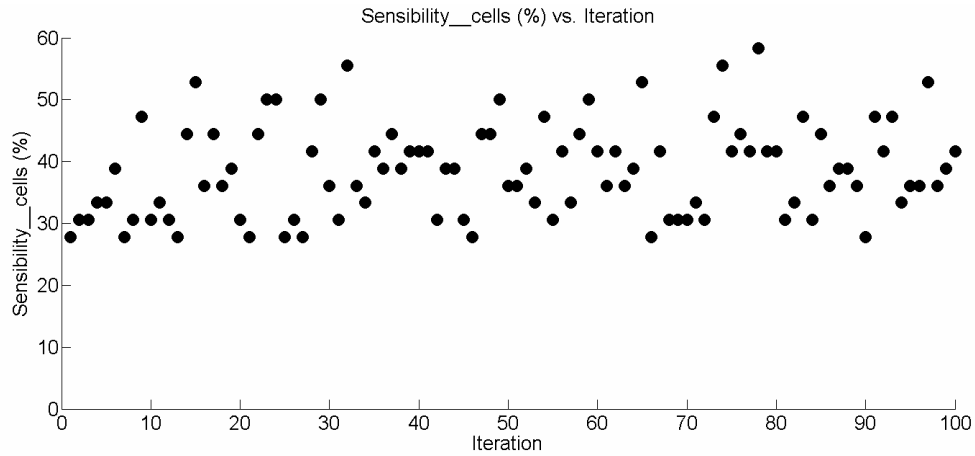

Figure 3.2: Graphic of Sensibility_cells η

The graphic in Figure 3.2 has underlined a randomness in clustering process, which has represented one of the problems faced in the subsequent phases of algorithm upgrading.

Even the FP_{cells} (number of cells recognized centromeres when the image is not centromere) has been drawn: the result is showed in Figure 3.3.

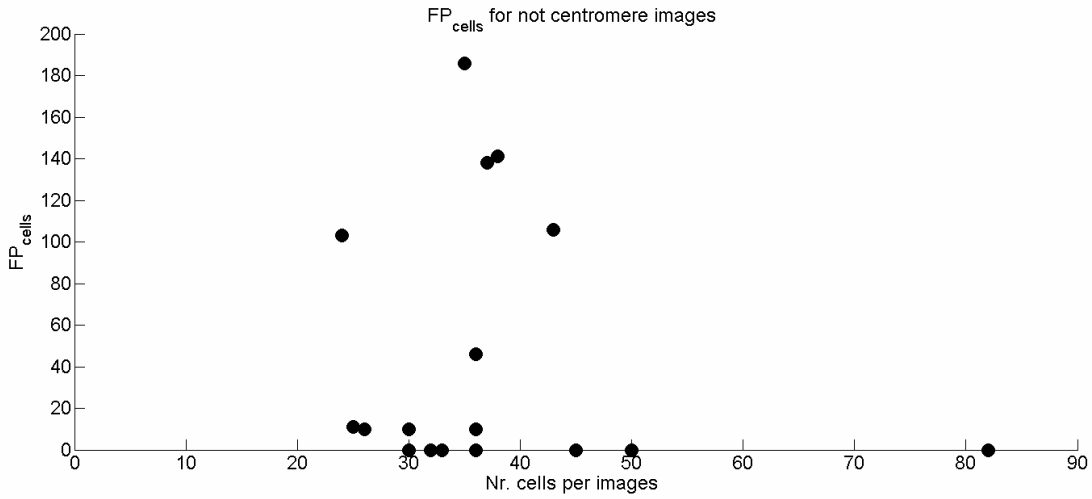

Figure 3.3: Graphic of FP_{cells} for not centromere images

The expected result was FP_{cells} = 0, but the graphic showed that the number of centromere cells found in not centromere images was too high: observing one of the images used to obtain this graphic (Figure 3.4 a), it's possible to note that the first version of the algorithm was really influenced by the noise present in the image (Figure 3.4 b), as a consequence of an over segmentation.

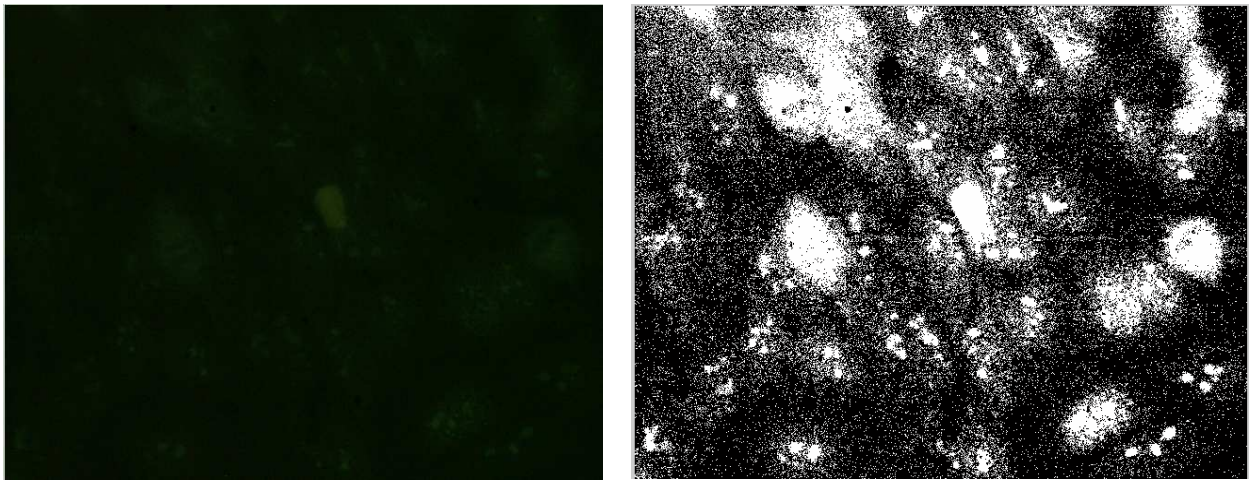

a) **b)**

Figure 3.4. a) Original nucleolar image; b) Segmented image

FP_{images} (the number of images recognized centromeres when the image is not centromere) was evaluated for every pattern different from centromere. As example is showed in Figure 3.5 the FP_{images} for nucleolar pattern which was dependent from CUT.

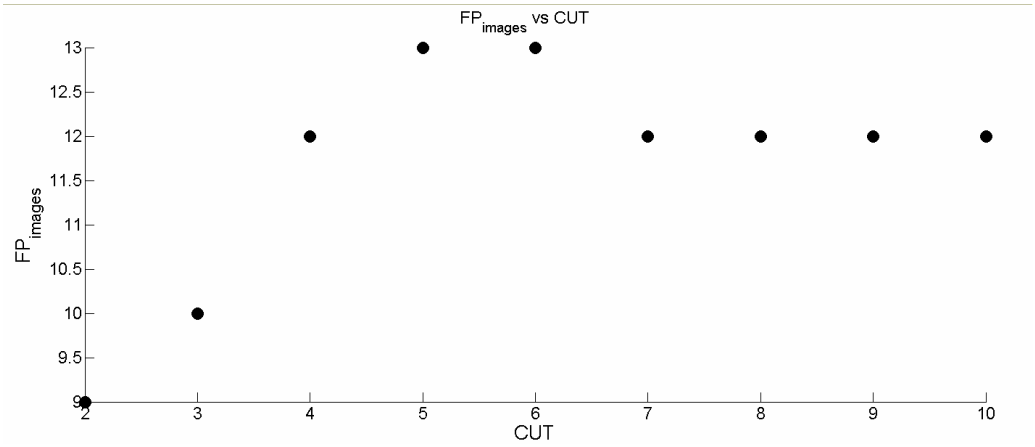

Figure 3.5: Graphic of FP_{images} for nucleolar pattern vs. Cut

Finally, to test the segmentation properties of the algorithm, it was depicted for centromere images the number of segmented objects (representing the centromeres) versus the number of cells in the images (Figure 3.6). Since a centromere cell contains from 23 to 46 centromeres, starting with N cells in an image it is expected to visualize from N*23 to N*46 segmented objects. Graphics in Figure 3.6 show the proportionality region.

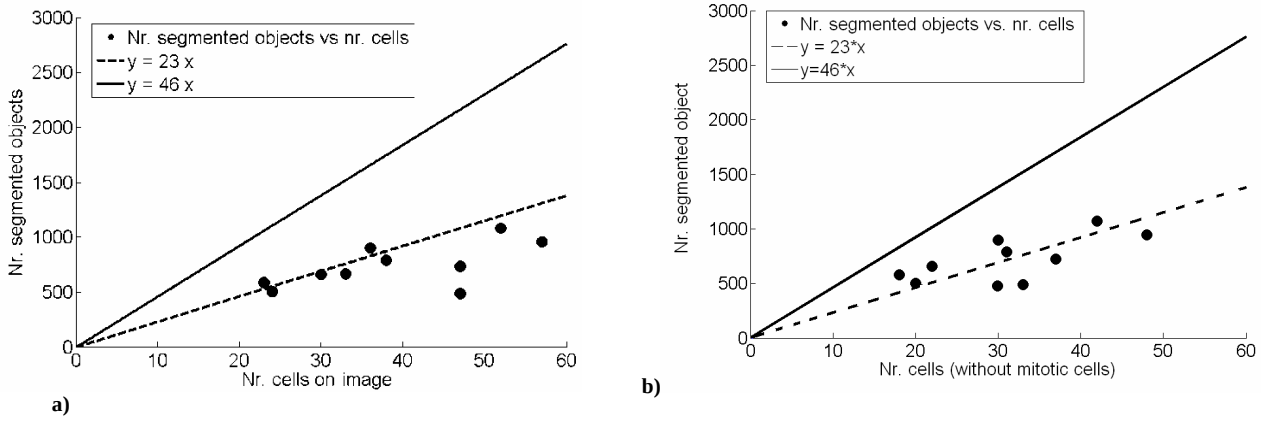

Figure 3.6: Graphic of nr. of segmented objects vs. nr. cells: a) with mitotic cells; b) without mitotic cells

The graphic in Figure 3.6 a) showed a bad proportionality between the number of cells presented in an image and the number of segmented objects and a different correlation from that expected; a first explanation probably comes from the presence in the images of mitotic cells, labelled by the algorithm as a single object (like a centromere) (Figure 3.7 a and b). In fact, as a confirmation of this hypothesis, Figure 3.6 b) showed the graphic of Figure 3.6 a) obtained without mitotic cells.

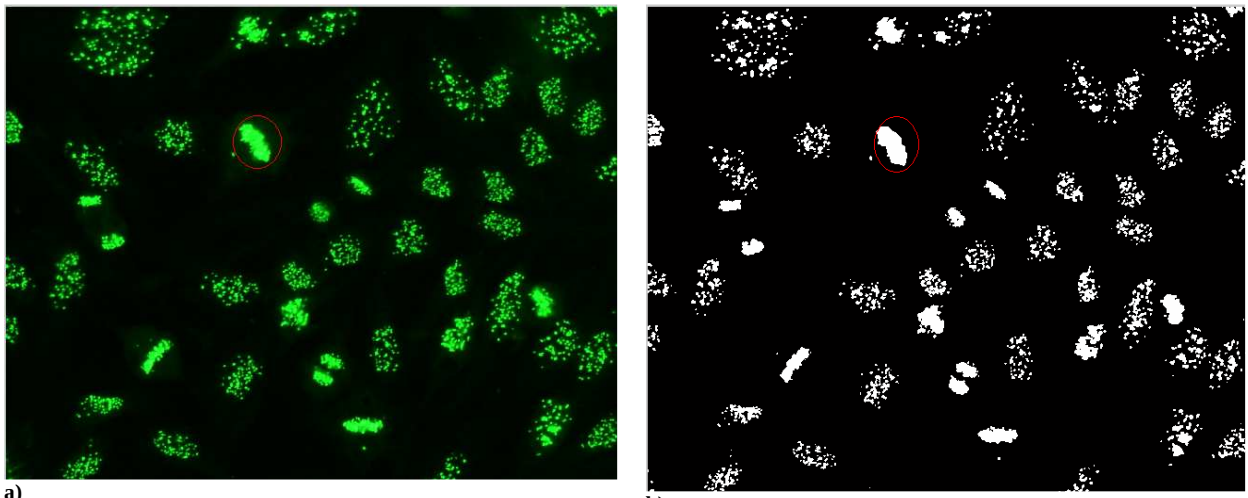

a) **b)**

Figure 3.7: A mitotic cell underlined in: a) Original centromere image; b) The same image after segmentation process

Anyway, mitotic cells cannot be removed from an image because their presence is characteristic of centromere patterns.

Considering this preliminary results, the subsequent modifications to the algorithm have concerned the elimination of the randomness from clustering process, the upgrade of the properties of segmentation and the noise reduction.

3.1.1 Algorithm revisions

The first problem to deal with was the randomness. As explained in paragraph 2.5, the K-means algorithm is an iterative algorithm which starts with a random partition selecting *c* points as initial seeds and assigning the objects to the closest center; then, new centers of clusters are calculated according to the equation 2.5.3 and the objects are assigned again until a minimum of the objective function is reached. So, performances of K-means algorithm depend on initial choice of centroids.

To overcome this problem a preprocessing phase was implemented.

The preprocessing phase, constituted, as already explained in paragraph 2.4, by a contrast adjustment algorithm followed by morphological operation, allowed to automatically underline and count the cells: the centroid of every cell was found and used as seed to K-means clustering.

To verify if the randomness has been removed, the Sensibility_cells η for centromere images was evaluated again, as in Figure 3.2, and the result is shown in Figure 3.8:

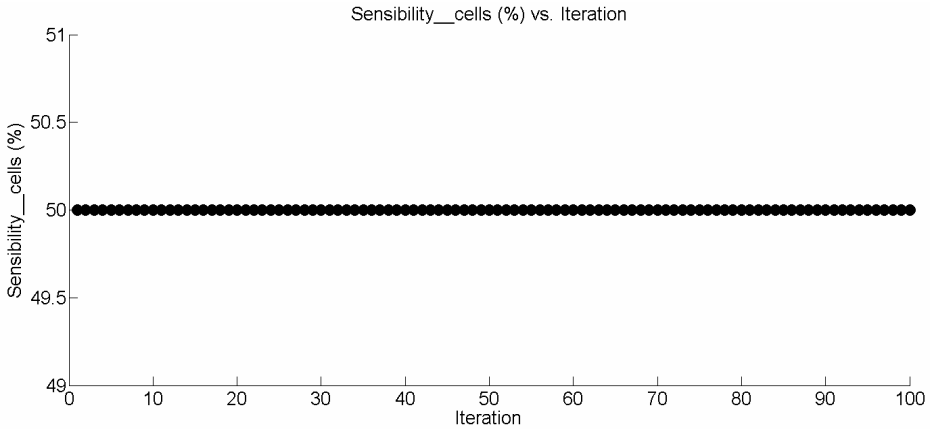

Figure 3.8: Graphic of Sensibility_cells η for a centromere image

It is possible to note that the number of centromere cells found on the image is constant, so using the position of cells as seeds for the K-means allowed to remove the randomness.

The preprocessing method, with the contrast-limited adaptive histogram equalization and the following operations, allowed also to remove the noise in the images. In fact, the originally threshold operation on images based on Otsu's method, which chooses the threshold to minimize the intraclass variance of the black and white pixels [90], wasn't able to segment correctly the cells and their centromeres.

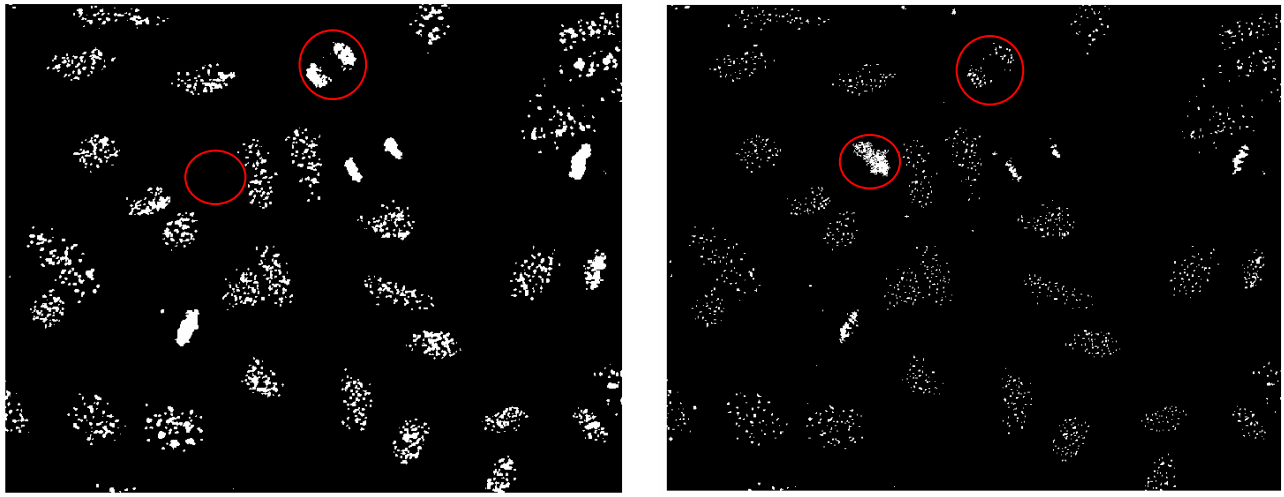

a) **b)**

Figure 3.9: a) Image segmented with Otsu's method; b) Image segmented with CLAHE method

Comparing Figure 3.9a and Figure 3.9b as example of the segmentation with Otsu's method and with CLAHE method respectively, it is possible to note that applying CLAHE on an image allows to enhance centromeres and to distinguish better mitotic cells.

It is possible to underline the advantages coming from the revised version of the algorithm also by showing the graphic of FP_{cells} obtained for not centromere images: representing on the same graph in Figure 3.10 the results obtained with the first version of the algorithm and the results obtained with the revised version of the algorithm it is possible to note that in the last case the FP_{cells} is near zero as expected.

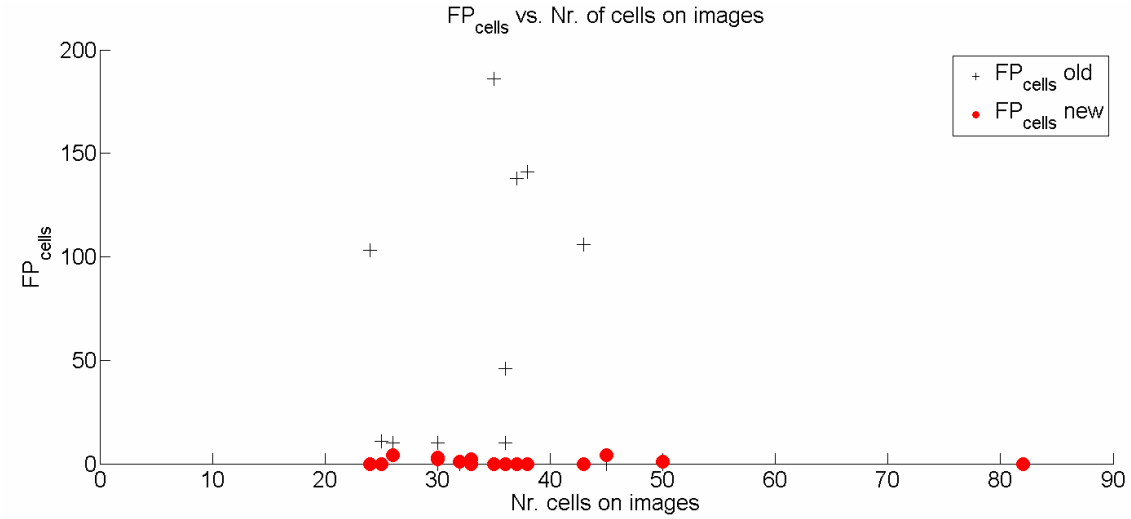

Figure 3.10: Comparison between the FP_{cells} obtained wih the old and the modified algorithm

Regarding the segmentation properties of the algorithm, we remember that the graphic in Figure 3.6a had showed a bad proportionality between the number of cells presented in an image and the number of segmented objects and a correlation different from that expected. In the upgrade version of the algorithm, the segmentation method was modified: as already explained, the application of the contrast-limited adaptive histogram equalization (CLAHE) with the morphological operations (dilation and holes filling), allowed to segment correctly the cells and their centromeres. Valuing again the number of segmented objects versus the number of cells in an image, we obtain the result shown in Figure 3.11.

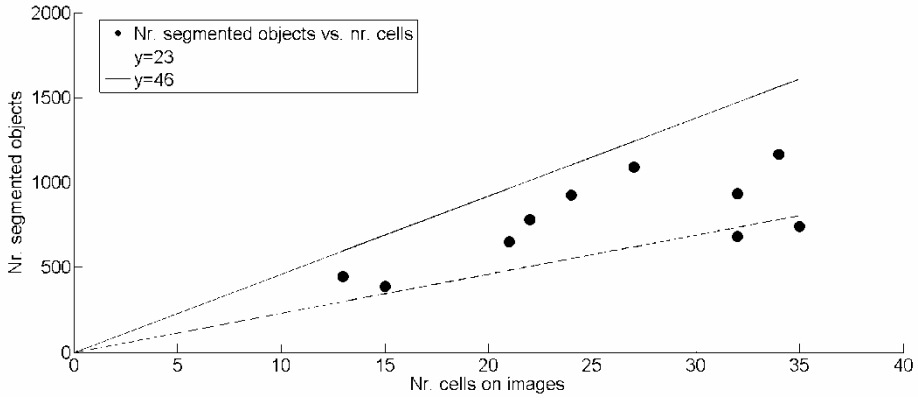

Figure 3.11: Graphic of nr. of segmented objects vs. nr. of cells

The Figure 3.11 shows the expected proportionality between the number of segmented objects (the centromeres) and the number of cells in an image.

3.1.2 Tuning phase

The selected database of Table 3.1 has been also used to extract and tune all useful parameters of the algorithm.

As described in paragraph 2.4, after the contrast adjustment of images and the morphological operations, on images objects smaller than a cells are present (Figure 3.12) coming form segmentation process.

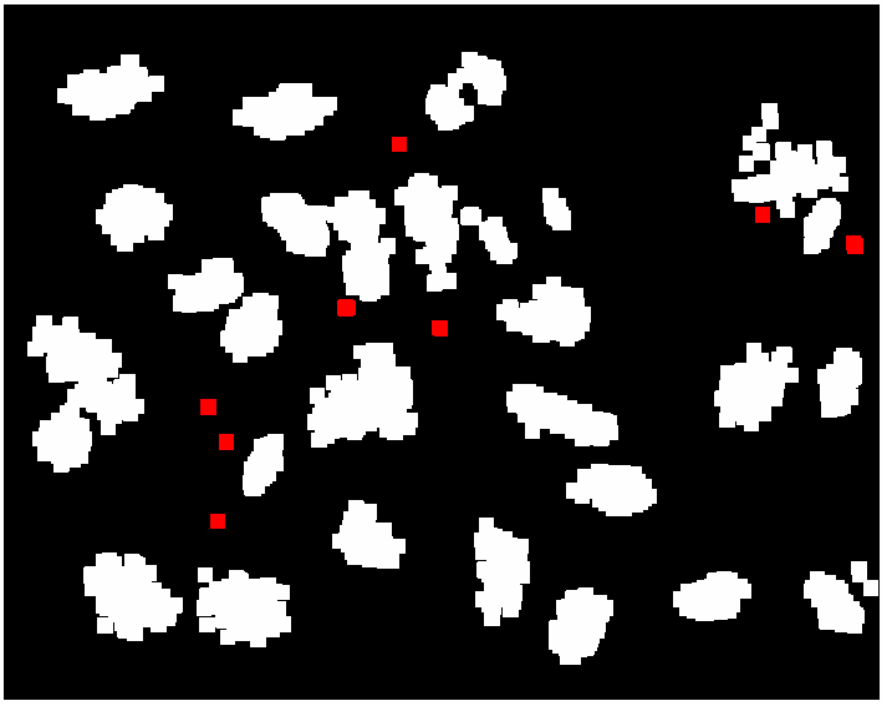

Figure 3.12: Example of image after preprocessing phase: small objects are visible

These objects may create many problems in the following phase of the process, because they can be erroneously considered like centromeres, so they have to be removed. To this purpose, the area (i.e. the number of pixels) of all objects in all images was evaluated, obtaining the following plot (Figure 3.13):

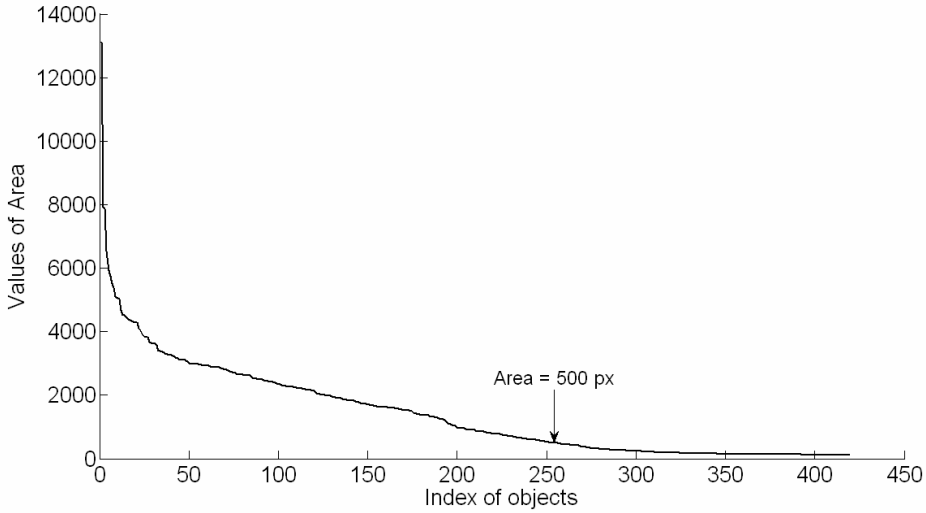

Figure 3.13: Plot of Area of all objects in the images

Observing the plot of the values of Area, an Area = 500 px is chosen as threshold: regions smaller than this threshold are removed obtaining the image shown in Figure 3.14

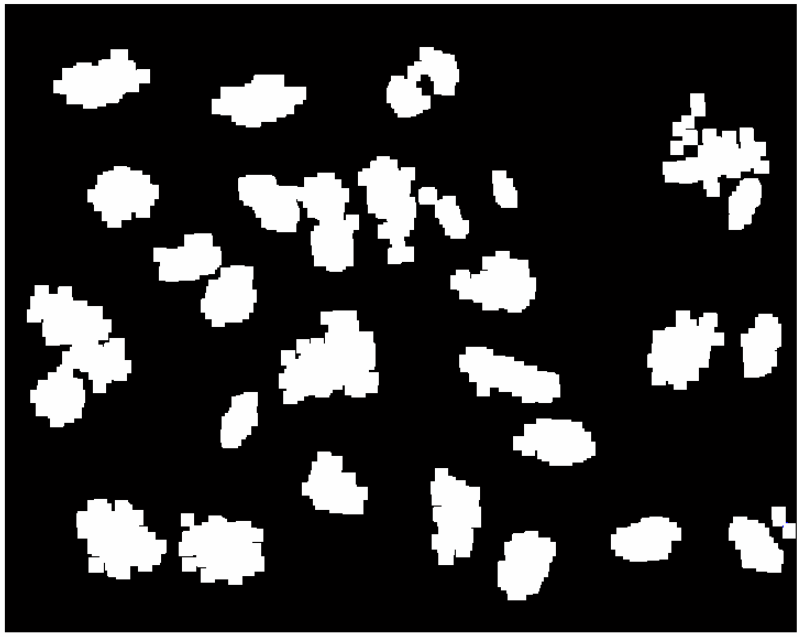

Figure 3.14: Image after the remotion of small objects

After the elimination of small objects, from the cells remained in images (see Figure 3.14) the *eccentricity* has been extracted: this parameter is the ratio of the distance between the foci of the ellipse having the same second-moments as the region and its major axis length. The value is between 0 and 1: an ellipse whose eccentricity is 0 is actually a circle, while an ellipse whose eccentricity is 1 is a line segment. The eccentricities distribution is shown in Figure 3.15.

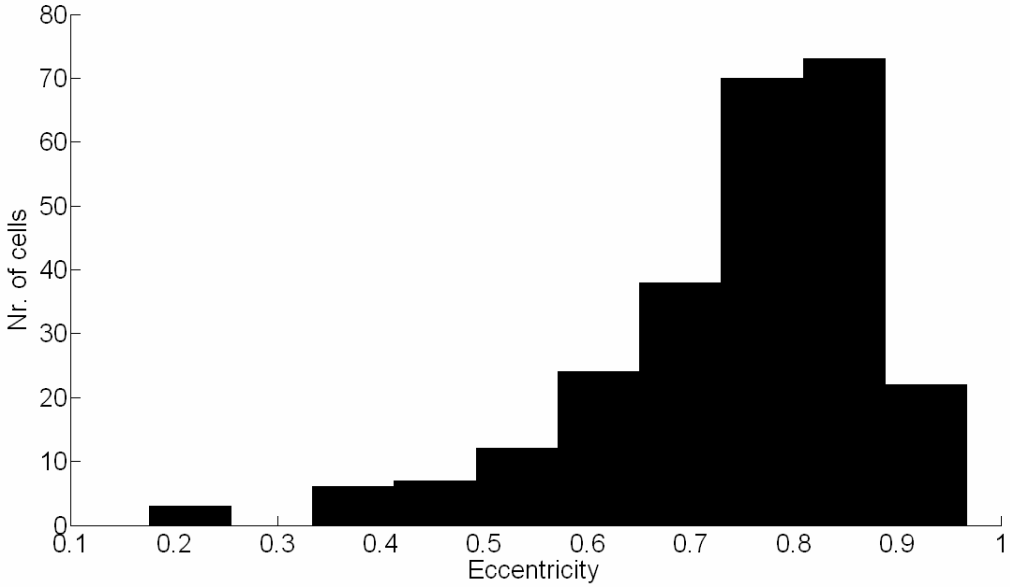

Figure 3.15: Histogram of eccentricities

The mean value of eccentricities with its standard deviation is:

$$\text{eccentricity}_{\text{mean}} = (0.74 \pm 0.14)$$

The results suggested that the cells have an ellipsoidal form, so a scalar specifying the length (in pixel) of the Major Axis of the ellipse has been extracted from all regions. This parameter is used as control parameter for the clustering process: in fact, even if a cluster contains the correct number centromeres, its dimension cannot overcome that of a centromere cells.

The distribution of the major axis lengths is showed in Figure 3.16. The mean value of major axis lengths, chosen as control parameter, with its standard deviation is:

$$\text{Major axis length}_{\text{mean}} = (65 \pm 30)\ \text{px}$$

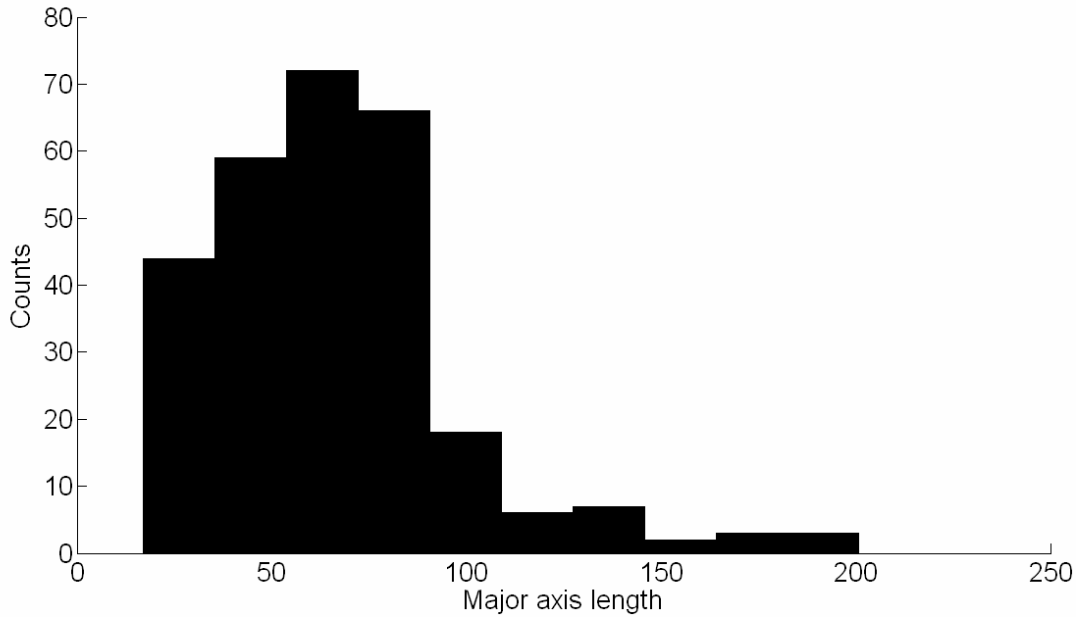

Figure 3.16: Histogram of major axis lengths

Finally, observing the graph of Sensibility_images ε versus the parameter CUT (Figure 3.1), we fixed for the testing phase the parameter CUT = 5. because for highest values the Sensibility starts to decrease.

3.2 Results and Discussion

After the revision and the tuning processes, it has been possible to test the algorithm on the entire dataset acquired thanks to the A.I.D.A. project. Indeed, the algorithm has been tested also on the public database present on the http://mivia.unisa.it website.

3.2.1 Results of test on A.I.D.A. database

To test the proposed algorithm we used the figures of merit defined in paragraph 2.6:

$$\text{Sensibility\_images } \varepsilon = \frac{\text{number of images recognized centromere}}{\text{total of centromere images}}$$

$$\text{Sensibility\_cells } \eta = \frac{\text{number of cells recognized centromere}}{\text{total of cells}}$$

FP_{images} =number of images recognized centromeres (when the image is not centromere)

FP_{cells} = number of cells recognized centromeres (when the image is not centromere)

$$\text{Accuracy} = \frac{TP + TN}{TP + TN + FP + FN}$$

The database for the testing phase contains the following images (Table 3.2):

Table 3.2: List of images used for the test set

PATTERN	NUMBER OF IMAGES
Centromere	41
Coarse Speckled	74
Fine Speckled	111
Nuclear Homogeneous	308

Few Nuclear Dots	19
Nucleolar Clumpy	32
Nucleolar Homogeneous	40
Nucleolar Speckled	3
Other	65

The recognition of *n* centromere images over *N* real centromere images is referable to a binomial distribution characterised by a probability p defined as:

$$\mathrm{p} = \frac{n}{\mathrm{N}}$$

In our case, the probability p is the Sensibility, less than 1, and *n* is the number of centromere images (or cells) correctly selected by the doctor. So, the associated error to the expected value *n* is

$$\sigma_n = \sqrt{Np(1-p)}$$

And then to the Sensibility is associated the error

$$\sigma_p = \sqrt{\frac{p(1-p)}{N}}$$

The value of Sensibility_images, i.e. the number of centromere images correctly recognized, is

$$\text{Sensibility\_images } \varepsilon = 37/41 = (\mathbf{90 \pm 5})\ \%$$

The Sensibility_cells η was evaluated for each centromere image and the result is depicted in Figure 3.17.

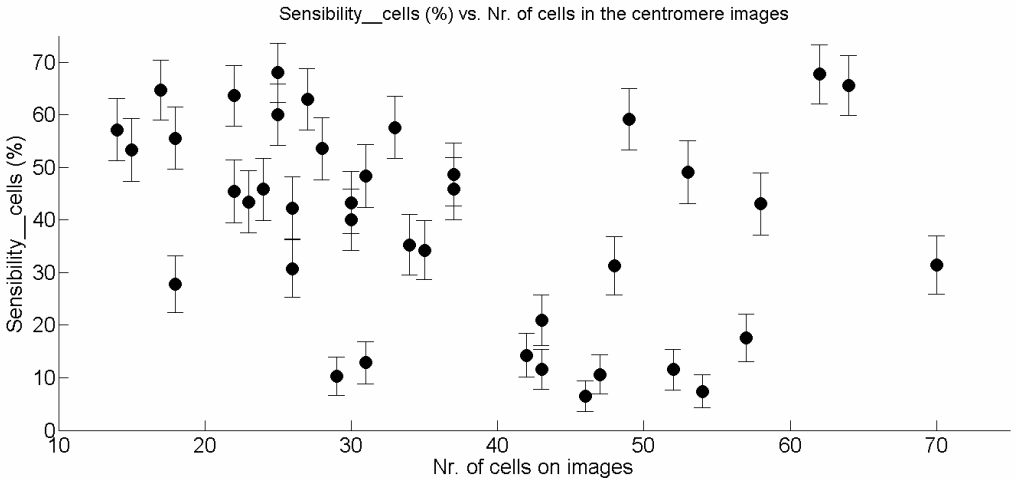

Figure 3.17: Graph of Sensibility_cells for centromere images

It is possible to note in Figure 3.17 that the Sensibility_cells values range over an interval starting from about 5% to 70%.

To understand how a different choice of parameter CUT may determine a variation in the Sensibility, we show in Figure 3.18 the graph of Sensibility_cells with a polygonal going through the value relative to a fixed number (equal to the value of CUT) of 5 recognized centromere cells in each image.

This polygonal allows to separate two regions: the region A, above the polygonal, to which belong all the centromere images correctly classified, and the region B, below the polygonal, to which belong all the centromere images lost.

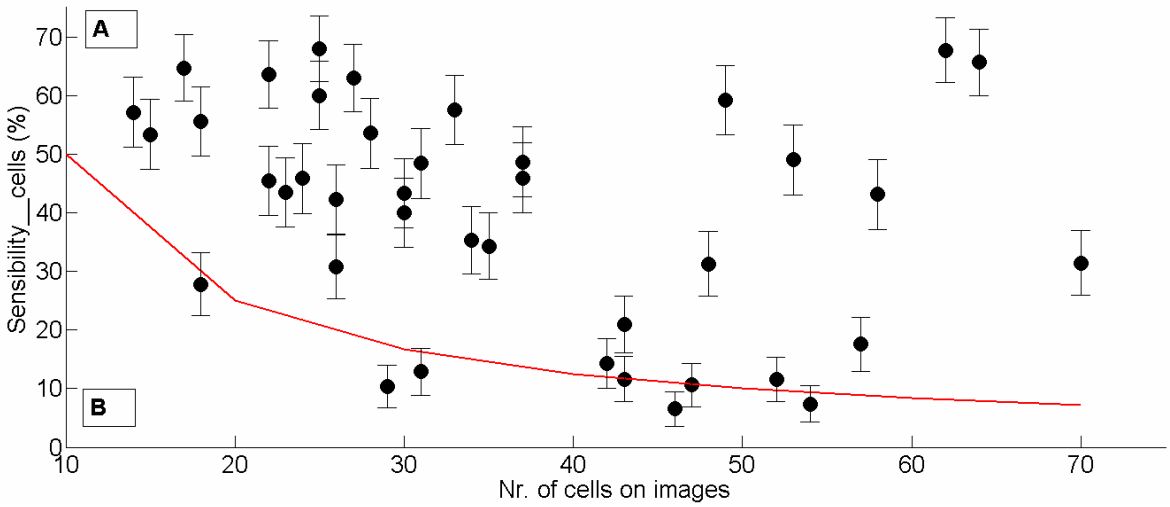

Figure 3.18: The Sensibility_cells for centromere images with the polygonal relative to 5 recognized centromere cells in each image

Then, a variation in the value of parameter CUT may increase or decrease the number of centromere images correctly classified and as a consequence the Sensibility of the method, as it is possible to understand even thanks to the Figure 3.19 in which it is shown directly the number of centromere cells found in each image with the straight line correspondent to a CUT = 5, which is the value chosen as threshold for classify an image as centromere.

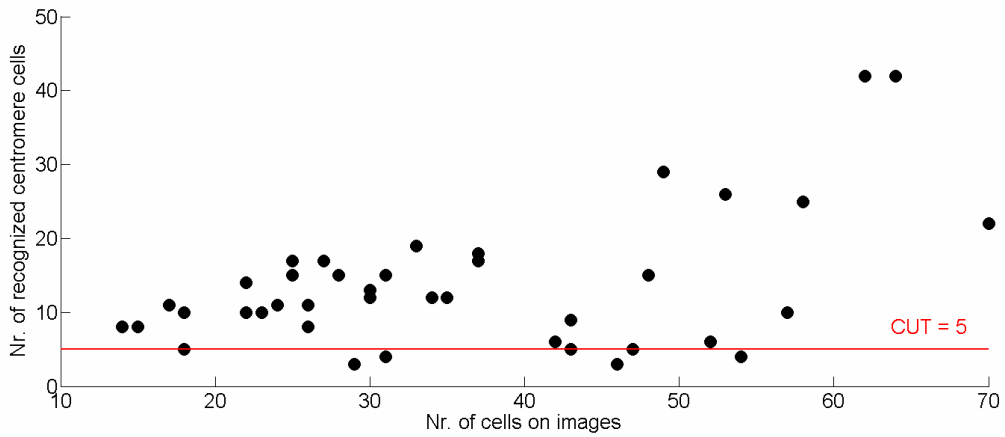

Figure 3.19: Graphic of the number of recognized centromere cells in each image with the straight line relative to CUT = 5

The values of FP_{cells} for not centromere images are indicated in the Table 3.3.

Table 3.3: Values of FP_{cells}

PATTERN	FP_{cells}
Coarse Speckled	69 (on 2095 cells)
Fine Speckled	38 (on 2012)
Nuclear Homogeneous	74 (on 8773)
Few Nuclear Dots	0 (on310)
Nucleolar Clumpy	0 (on 494)
Nucleolar Homogeneous	0 (on 909)
Nucleolar Speckled	0 (on 56)
Other	157 (2159)
All	338 (on 16808)

The FP_{images} are evaluated for every pattern different from centromere and for all patterns. The results are reported in the Table 3.4:

Table 3.4: Values of FP_{images}

PATTERN	**FP_{images}**
Coarse Speckled	3 (on 74 images)
Fine Speckled	1 (on 111)
Nuclear Homogeneous	1 (on 308)
Few Nuclear Dots	0 (on 19)
Nucleolar Clumpy	0 (on 32)
Nucleolar Homogeneous	0 (on 40)
Nucleolar Speckled	0 (on 3)
Other	6 (on 65)
All	11 (on 588)

The last figure of merit evaluated is the Accuracy for images, whose value is:

$$\text{Accuracy} = (98.0 \pm 0.5)\ \%$$

In which the error is calculated with the formula

$$\sigma_p = \sqrt{\frac{p(1-p)}{N}}$$

3.2.1 Results of test on MIVIA public database

The method was tested also on the MIVIA public database, present on the http://mivia.unisa.it website, an annotated database of IIF images, acquired using slides of HEp-2 substrate at the fixed dilution of 1:80, as explained in Paragraph 2.3.

The results of application of the method have been compared with the results of the first edition of the HEp-2 Cells Classification Contest held at the International Conference on Pattern Recognition in 2012, which focused on Indirect Immunofluorescence (IIF) image analysis: 28 different recognition systems able to automatically recognize the pattern of cells within IIF images were tested on the same undisclosed dataset [93]. In this occasion, the MIVIA database was divided in training set and test set according to the Table 3.5, and our proposed method was tested on the images belonging to the test set only.

Table 3.5: Number of images (cells) for the training set and the test set

	Training set	**Test set**
Centromere	3	3 (*149*)
Coarse Speckled	2	3 (*101*)
Fine Speckled	2	2 (*114*)
Homogeneous	3	2 (*180*)
Nucleolar	2	2 (*139*)
Cytoplasmatic	2	2 (*51*)

The participants to the Contest received the training set with the original images of the cells already segmented by specialists. Then, the participants used the training set to tune their HEp-2 cells classification system and then they released the executable for the independent evaluation on the test set. Finally, they ran all the submitted executables on the test set collecting the results.

Our method instead automatically segments the cells in all images, obtaining the same number of cells almost in the same location of that segmented manually by the specialists of the Contests, as it is possible to observe in the Figure 3.20.

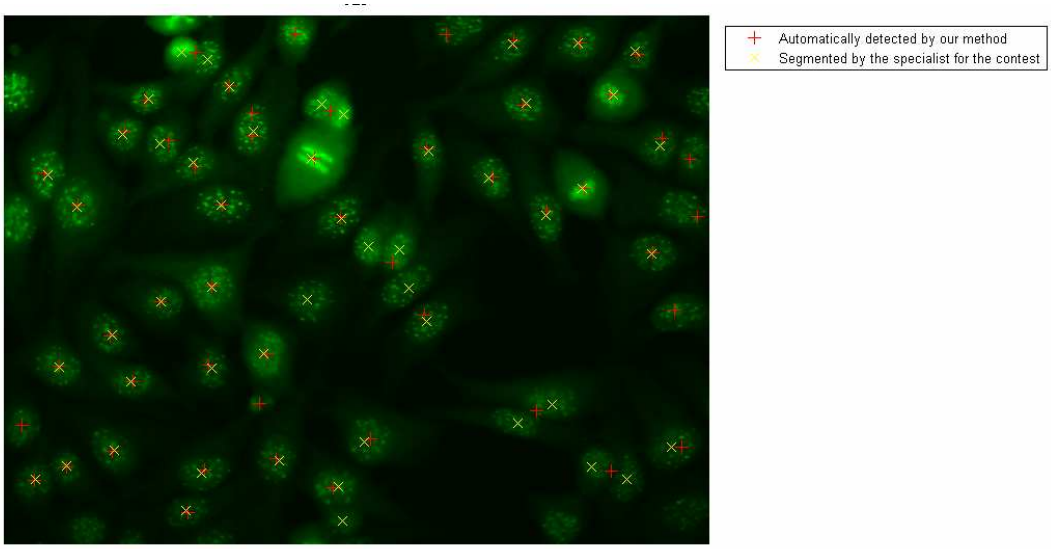

Figure 3.20: Comparison between the position of the cells found by the proposed method and by the specialists

Since our method allows to recognize the centromere pattern, only the results of the Contest regarding the centromere pattern will be considered in the following.

To verify the properties of the proposed algorithm the figures of merit Sensibility_cells has been evaluated. The figure of merit Sensibility_images has not been considered here because the algorithms of the Contest are algorithm of cells recognition. Anyway, according to our parameter, our algorithm allows to recognize all the centromere images of the test set.

Moreover, according to the HEp-2 Contest, even the figure of merit Accuracy, defined as

$$\text{Accuracy} = \frac{TP + TN}{TP + TN + FP + FN}$$

has been evaluated.

The value of Sensibility_cells η for centromere images of the test set for our algorithm is:

$$\text{Sensibility\_cells } \eta \text{ (centromere images)} = (66 \pm 4)\ \%$$

The Figure 3.21 shows the Centromere cells Sensibility achieved by all the considered methods.

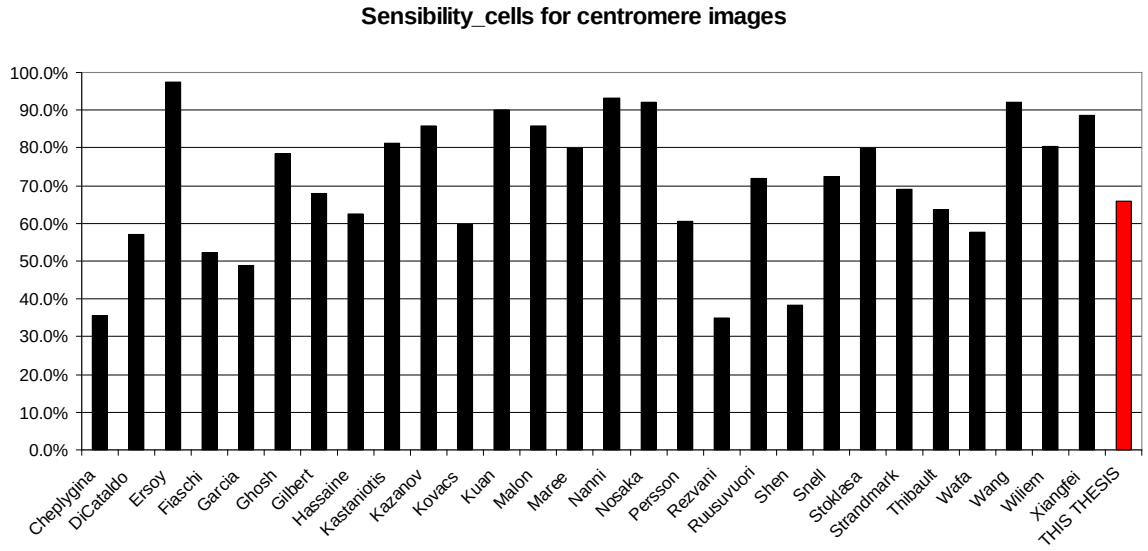

Figure 3.21: The Centromere cells Sensibility on the test set for all the methods

The values of FP_{cells} e FP_{images} for our algorithm are indicated in the Table 3.6.

Table 3.6: Values of FP_{cells} and FP_{images}

	FP_{cells}	**FP_{images}**
Coarse Speckled	0 (on 101 cells)	0 (on 3 images)
Fine Speckled	0 (on 114)	0 (on 2)
Homogeneous	0 (on 180)	0 (on 2)
Nucleolar	0 (on 139)	0 (on 2)
Cytoplasmatic	8 (on 51)	1 (on 2)
All	8 (on 585)	1 (on 11)

The value of Accuracy is:

$$\text{Accuracy} = (92 \pm 1)\ \%$$

The Figure 3.22 shows the centromere cells recognition accuracy achieved by all the considered methods.

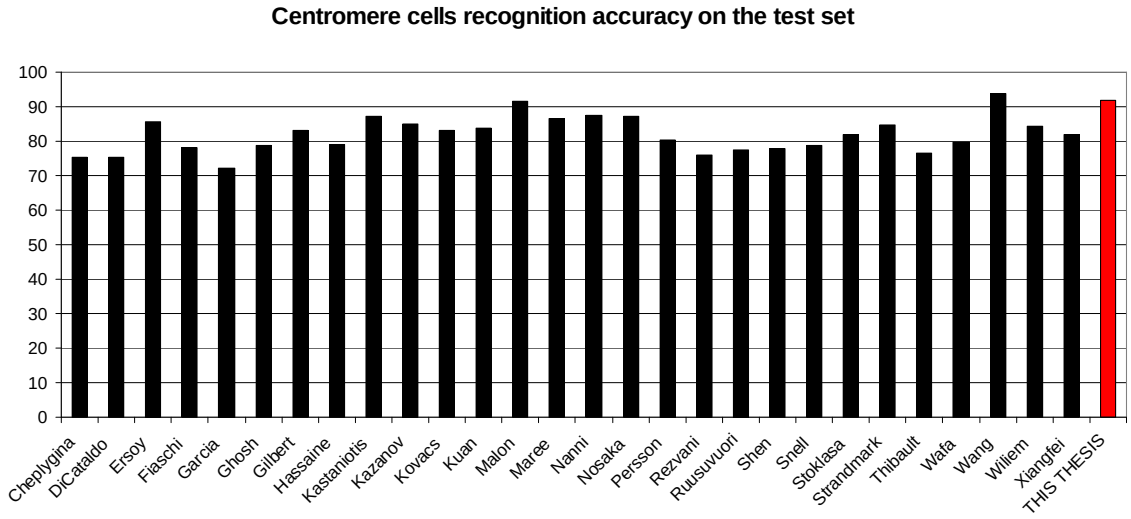

Figure 3.22: The Centromere cells recognition accuracy on the test set obtained by all the methods

It is possible to note that the value of Accuracy obtained by our method is comparable with the best results of the contest. It is important underline, however, that our method automatically segment and count the cells present in the images, while the participants to the contest received the training set with the cells already segmented.

Conclusions and perspectives

The aim of this study was to develop an automated method of centromere pattern recognition to support the IIF diagnosis of autoimmune diseases. The proposed method is based on the grouping, through a clustering algorithm, of the fluorescent centromeres present on the cells.

After a phase of preliminary testing useful to show some initial problems, the corrected and improved version of the method was tested on the database of IIF images collected thanks to the project A.I.D.A. and on a public database present on the http://mivia.unisa.it website.

The performances of our method was evaluated through the following figures of merit:

$$\text{Sensibility\_images } \varepsilon = \frac{\text{number of images recognized centromere}}{\text{total of centromere images}}$$

$$\text{Sensibility\_cells } \eta = \frac{\text{number of cells recognized centromere}}{\text{total of cells}}$$

FP_{images} =number of images recognized centromeres (when the image is not centromere)

FP_{cells} = number of cells recognized centromeres (when the image is not centromere)

$$\text{Accuracy} = \frac{TP + TN}{TP + TN + FP + FN}$$

The results of the test on the A.I.D.A. database showed a Sensibility_images of (90 ± 5)%, a Sensibility_cells variable in the interval [5%, 70%], a FP_{cells} of 338/16808 and a FP_{images} of 11/588; the value of Accuracy was (98.0 ± 0.5)%.

The results of the test on the MIVIA database showed a Sensibility_cells of (66 ± 4) % for all centromere images, a FP_{cells} of 8/585 and a FP_{images} of 1/11. The value of Accuracy was (92 ± 1) %.

Comparing these results with the results obtained on the same database by the participants to the HEp-2 Contest it is possible to note that our method has a centromere cells recognition Accuracy comparable with the three best values obtained by participants. Indeed, it is important underline that our method allows an automatic segmentation and counting of the cells present in the images, while the participants to the contest received the training set with the original images of the cells already segmented by specialists.

Moreover, it is important to underline that the proposed method achieved encouraging results on AIDA database and on MIVIA database considering only the centromeres position as feature for the K-means, i.e., making clusters only in the Euclidean space.

Being based on these considerations, one of the aim of future works will be to increase the number of features to further improve the results.

To make the proposed method suitable for application in a CAD system, it will be necessary to test and apply it on pattern different from centromere. One of the next application will concern the nucleolar pattern, characterised by large coarse speckled staining within the nucleus, from four to six in number per cell.

Moreover, other classification methods will be tested and compared, like neural networks or support vector machines, trying to use them even in parallel to make faster the process of pattern recognition.

Appendix A: Structure of HEp-2 cells

Immunofluorescence patterns seen on individual HEp-2 cells are related to the cell cycle. For instance, patterns that are unique to cells in mitosis will be restricted to cells in that phase of the cycle. Since most patterns are seen with cells in interphase, HEp-2 cells should be largely at this stage. In interphase, the chromosomes form a fibrillar network of chromatin, more or less uniformly distributed throughout the nucleoplasm and delimited by the nuclear membrane. Only the nucleoli are well differentiated. Cytoplasmic organelles and fibrous structures are most visible at this stage and tend to largely disappear or change their appearance during mitosis (Figure A.1).

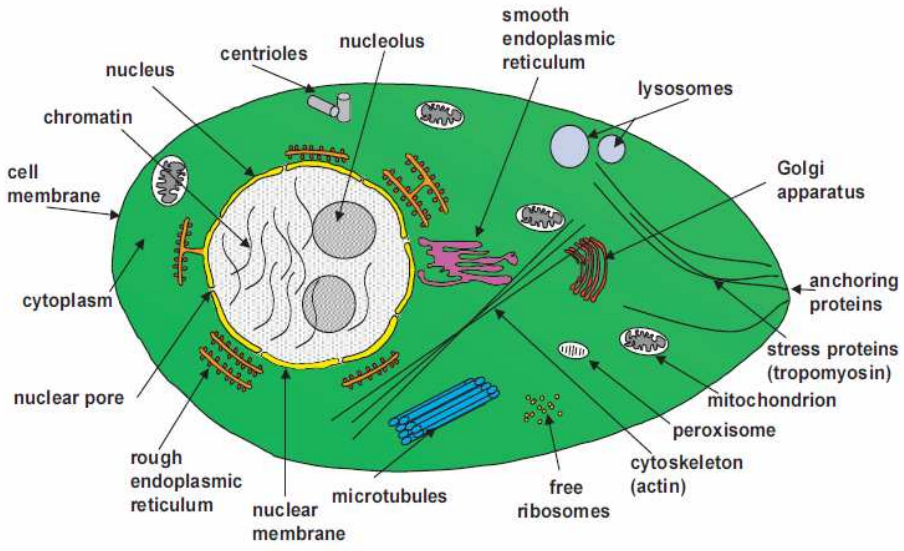

Figure A.1: The cell during the interphase

The nuclear envelope is the membrane that maintains the integrity of the nucleoplasm during interphase. The endoplasmic reticulum is an extension of this envelope, which projects into the cytoplasm. There are three distinct layers: the nuclear lamina, the inner and the outer nuclear membranes. Linked to these are nuclear pore complexes and the ribosomes are attached to the rough endoplasmic reticulum.

Mitosis occurs during 10% - 15% of the cell cycle and is divided into five successive phases: prophase, prometaphase, metaphase, anaphase and telophase.

During prophase, DNA condensation gives rise to the appearance of individual chromosomes whilst the nucleolar contents are distributed throughout the nucleoplasm. Meanwhile, the mitotic spindle forms around the nucleus and terminates at the polar centrioles (or centrosomes). The mitotic spindle is composed of microtubules and associated proteins.

During prometaphase, the nuclear membrane disrupts and then disappears. The chromosomes attach to the mitotic spindle via the kinetochores which have formed on the chromosome centromeres.

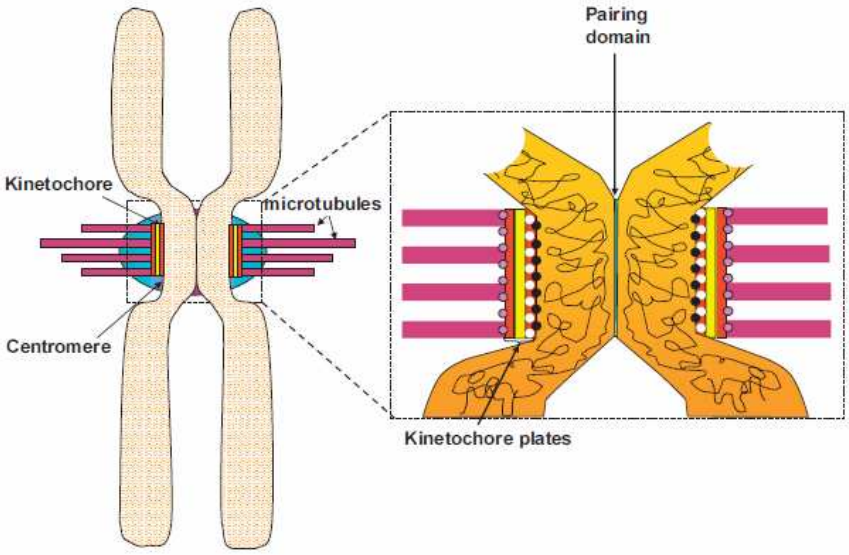

Figure A.2: Diagram showing the location of the centromere proteins

Metaphase is characterised by the localisation of condensed chromosomes at the equatorial plane of the spindle apparatus through the action of microtubules.

In anaphase, each pair of chromatids splits at the centromere and the chromatids migrate separately to each pole of the spindle. Microtubules disappear at the end of anaphase as the chromatids reach opposite poles of the mitotic spindle.

In telophase the nuclear membrane re-forms around each of the two daughter nuclei. The nucleoli reappear and the chromosomes become decondensed in the newly re-formed nuclei.

The centromere pattern is characterised by several discrete speckles distributed throughout the interphase nuclei and characteristically found in the condensed nuclear chromatin during mitosis as a bar of closely associated speckles. The pattern is primarily found in CREST syndrome (Calcinosis, Raynaud's phenomenon, Esophageal dysmotility, Sclerodactyly and Telangiectasias), a mild variant of progressive systemic sclerosis of which approximately 55% are anti-centromere antibody (ACA) positive. The centromere proteins are located at the inner and outer kinetochore plates (Figure A.2), which interact with the mitotic spindle apparatus during mitosis.

Appendix B: Morphological operations

Mathematical morphology is a tool for extracting image components useful in representation and description of region shape. The language of mathematical morphology is set theory: sets in mathematical morphology are objects of an image. In fact, some basic concepts of morphological operation are based on operation coming from the set theory.

The two principal morphological operations are **dilation** and **erosion**. These operations are fundamental to morphological processing since many of the morphological algorithm are based on these two primitive operations [3]. Dilation allows objects to expand, thus potentially filling in small holes and connecting disjoint objects (Figure B.1).

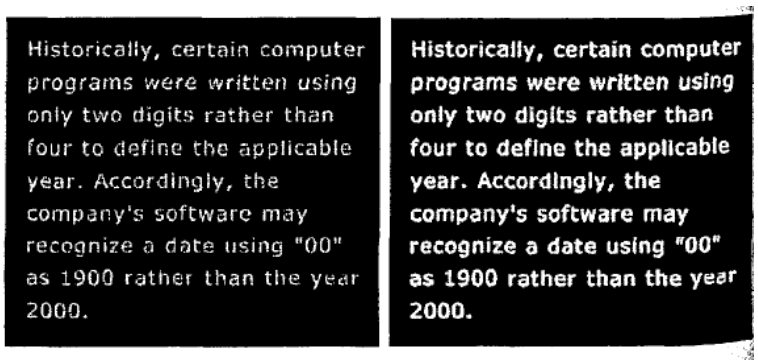

a) **b)**

Figure B.1: Example of dilation operation: a) Input image containing broken text; b) Dilated image

Erosion shrinks objects by etching away (eroding) their boundaries (Figure B. 2).

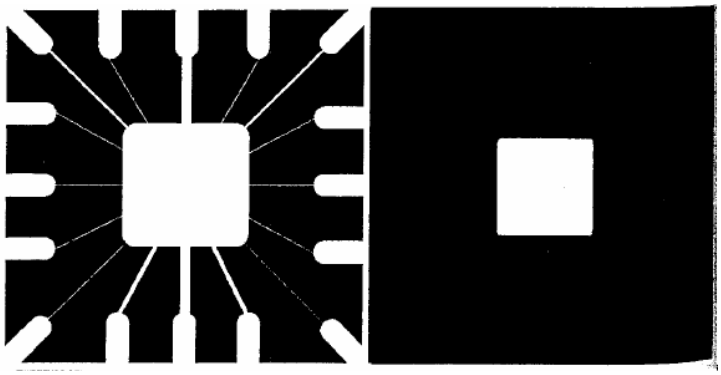

a) **b)**

Figure B. 2: Example of erosion operation: a) original image; b) eroded image

These operations can be customized for an application by the proper selection of the structuring element, which determines exactly how the objects will be dilated or eroded.

These two basic operations, dilation and erosion, can be combined into more complex sequences. The most useful of these for morphological filtering are called **opening** and **closing** [92]. Opening consists of an erosion followed by a dilation and can be used to eliminate all pixels in regions that are too small to contain the structuring element, closing consists of a dilation followed by erosion and can be used to fill in holes and small gaps (Figure B.3).

a) **b)** **c)**

Figure B.3: a) Original image; b) Opening of a; c) Closing of a

The order of operation is important. Closing and opening will generate different results even though both consist of erosion and dilation.

When dealing with binary images, the principal application of morphology is extracting image components that are useful in the representation and description of

shape. In particular, it is possible to consider morphological algorithm for extracting boundaries or for region filling.

For example, the boundary of a set A can be obtained by first eroding A by a suitable structuring element and then performing the set difference between A and its erosion.

An operation of region filling is based on set dilation, complementation and intersection.

The majority of application of morphological concepts involve binary images; anyway, it is possible to extend the basic operations of dilation, erosion, opening and closing to grey-scale images too.

List of figures

Chapter 1

Chapter 2

Chapter 3

Appendix A

Appendix B

List of tables

Chapter 2

Chapter 3

References

[1] Morton M. J., Whaley D. H., Brandt K. R., Amrami K. K., Screening mammograms: interpretation with computer-aided detection – Prospective evaluation, 239 (2) 375-383 (2006)

[2] Ginneken B., Schaefer – Prokop C., Prokop M., Computer – Aided diagnosis: how to move from the laboratory to the clinic, Radiology, 261, 3 (2011)

[3] Digital Image Processing, William Pratt, John Wiley & Sons, 2001

[4] Dhawan A. P., Buelloni G., Gordon R., Enhancement of mammographic features by optimal adaptive neighbourhood image processing, IEEE Trans. Med. Imag. MI 5 (1) (1986) 8–15.

[5] Kim J. K., Park J. M., Song K. S., Park H. W., Adaptive mammographic image enhancement using first derivative and local statistics, IEEE Trans. Med. Imaging 16 (5) (1987) 495–502.

[6] Karssemeijer N., Adaptive noise equalization and recognition of microcalcification clusters in mammograms, Int. J. Pattern Recognition Artif. Intell. 7 (6) (1993) 1357-1376

[7] Bedi S.S., Khandelwal R., Various Image Enhancement Techniques: A Critical Review, IJARCCE, Vol. 2, Issue 3 (2013)

[8] Maini R., Aggarwal H., A Comprehensive Review of Image Enhancement Techniques, J.O. Computing, Vol. 2, Issue 3 (2010)

[9] Saruchi, Lal M., Comparative Study Of Different Image Enhancement Techniques, IJCT, Volume 2 No. 3 (2012)

[10] Somasundaram S.K., Alli P., A review on recent research and implementation Methodologies on Medical Image Segmentation, J. Computer Sci., 8 (1): 170-174 (2012)

[11] P.Lakshmi Devi, S.Varadarajan, Image Segmentation and Techniques: A

Review, IJART, Vol. 1 Issue 2 (2011)

[12] Tripathi S., Kumar K., Singh B.K., Singh R.P., Image Segmentation: A Review, IJCSMR, Vol 1 Issue 4 (2012)

[13] Seerha G., Review on Recent Image Segmentation Techniques, IJCSE, Vol. 5 No 2 (2013)

[14] Shen L., Rangayyan R., Desautles J. E., Detection and classification of mammographic calcification, Int. J. Pattern Recognition Artif. Intell. 7, 1403-1416 (1993)

[15] Lefebvre F., Benali H., Kahn E., Paola R. D., A fractal approach to the segmentation of microcalcifications in digital mammograms ,Med. Phys. 22 (4) (1995) 381-391

[16] Chaudhuri B. B., Sarkar N., Texture segmentation using fractal dimension, IEEE Transactions on Pattern Analysis and Machine Intelligence 17 (1) (1995) 72-77

[17] Li H., Liu K. J. R., Lo S. B., Fractal modelling and segmentation for the enhancement of microcalcifications in digital mammograms, IEEE Trans. Med. Im. 16 (6) (1997) 785-798

[18] Strickland R. N., Hahn H. I, Wavelet transforms for detecting microcalcifications in mammography, Proceedings of the International Conference on Image Processing, 1994, pp 402-406

[19] Strickland R. N., Hahn H. I., Wavelet transform matched filters for the detection and classification of microcalcifications in mammography, Proceedings of the 1995 IEEE International Conference on Image Processing, October 23-28, 1995, pp. 422-425

[20] Lu D., Weng Q., A survey of image classification methods and techniques for improving classification performances, International Journal of Remote Sensing, Vol. 28, No. 5, 823–870 (2007)

[21] Chan H., Lo S. B., Sahiner B., Lam K., Helvie M. A., Computer-aided detection of mammographic microcalcification: Pattern recognition with an artificial neural network, Med. Phys. 22 (10), 1555-1567 (1995)

[22] Chan H., Sahiner B., Petrick N., Helvie M., Lam K., Adler D., Goodsitt M.,

Computerized classification of malignant and benign microcalcifications on mammograms: texture analysis using an artificial neural network, Phys. Med. Biol. 42, 549-567 (1997)

[23] Wu Y., Doi K., Giger M., Nishikawa r., Computerized detection of clustered microcalcifications in digital mammograms: application of artificial neural network, Med. Phys., 19 (3) 555-560 (1992)

[24] Brake G., Karssemeijer N., Hendriks J., An automatic method to discriminate malignant masses from normal tissue in digital mammograms, Phys. Med. Biol. 45, 2843-2857 (2000)

[25] Jiang Y., Nishikawa R., Wolverton D., Metz C., Giger M., Schmidt R., Vyborny C., Doi K., Malignant and benign clustered microcalcifications: automated feature analysis and classification, Radiology 198, 671-678 (1996)

[26] Papadopoulos A., Fotiadis D. I., Likas A., An automatic microcalcification detection system based on hybrid neural network classifier, Artificial Intelligence in Medicine 25, 149-167 (2002)

[27] McCulloch W. S., Pitt W., A logical calculus of the ideas immanent in nervous activity, Bulletin of Mathematical Biophysics, 5, 115-133 (1943)

[28] Giger M. L., Chang H. P., Boone J., Anniversary Paper: History and status of CAD and quantitative image analysis: the role of medical physics and AAPM, Med. Phys. 35 (12) 2008

[29] Doi K., Computer –aided diagnosis in medical imaging: historical review, current status and future potential, Computerized Medical Imaging and Graphics 31 198–211(2007)

[30] Karssemeijer N., Hendriks J., Computer-assisted reading mammograms, Eur. Radiol. 7, 743-748 (1997)

[31] Freer T. W., Ulissey M. J., Screening mammography with computer-aided detection: prospective study of 12860 patients in a community breast centre, Radiology, 220, 781-786 (2001)

[32] Ciatto S., Rosselli Del Turco M., Burke P., Paci E., Zappa M., Comparison of standard and double reading and computer-aided detection (CAD) of

interval cancers at prior negative screening mammograms: blind review, British Journal of Cancer, 89, 1645-1649 (2003)

[33] Astley S. M., Gilbert F. J., Computer-aided detection in mammography, Clinical Radiology, 59, 390-399 (2004)

[34] Shiraishi J., Li Q., Appelbaum D., Doi K., Computer-Aided Diagnosis and Artificial Intelligence in Clinical Imaging, Seminars in nuclear medicin, 41, 6 (2011)

[35] Heimann T. , van Ginneken B. , Styner M. A. , Comparison and evaluation of methods for liver segmentation from CT datasets, IEEE Trans Med Imaging 28 (8)1251 – 1265 (2009)

[36] Albanese A. , Hall C. , Stanhope R., The use of a computerized method of bone age assessment in clinical practice, Horm. Res., 44 2 – 7 (1995) .

[37] Giger M. L., Doi K., MacMahon H., Metz C. E., Yin F.-F., "Computer-aided detection of pulmonary nodules in digital chest images," Radiographics 10, 41–52 (1990)

[38] Kobayashi T., Xu X.-W., MacMahon H., Metz C. E., Doi K., "Effect of a computer-aided diagnosis scheme on radiologists' performance in detection of lung nodules on radiographs," Radiology 199, 843–848 (1996)

[39] MacMahon H., Engelmann R., Behlen F. M., Hoffmann K. R., Ishida T., Roe C., Metz C. E., and Doi K., "Computer-aided diagnosis of pulmonary nodules: Results of a large-scale observer test," Radiology 213, 723–726 (1999)

[40] Davies D. H., Dance D. R., Automatic computer detection of clustered microcalcification in digital mammograms, Phys. Med. Biol. 35 (1990) 1111-1118

[41] Nishikawa R., "Current status and future directions of computer-aided diagnosis in mammography," Comput. Med. Imaging Graph. 31, 224– 235 (2007)

[42] Vivona L., Cascio D., Magro R., Fauci F., Raso G., A Fuzzy Logic C-Means Clustering Algorithm to Enhance Microcalcifications Clusters in Digital Mammograms, Proceedings of the IEEE Nuclear Science

Symposium Conference (2011)

[43] Acar B., Beaulieu C. F., Gokturk S. B., Tomasi C., Paik D. S., Jeffrey R. B., Yee J., Napel S., “Edge displacement field-based classification for improved detection of polyps in CT colonography,” IEEE Trans. Med. Imaging 21, 1461–1467 (2002)

[44] Summers R. M., Jerebko A. K., Franaszek M., Malley J. D., Johnson C. D., “Colonic polyps: Complementary role of computer-aided detection in CT colonography,” Radiology 225, 391–399 (2002)

[45] Mani A., Napel S., Paik D. S., Jeffrey R. B., Yee J., Olcott E. W., Prokesch R., Davila M., Schraedley-Desmond P., Beaulieu C. F., “Computed tomography colonography: Feasibility of computer-aided polyp detection in a ‘first reader’ paradigm,” J. Comput. Assist. Tomogr. 28, 318–326 (2004)

[46] Bossuyt X., Cooreman S., De Baere H., Detection of antinuclear antibodies by automated indirect immunofluorescence analysis, Clinica Chimica Acta international journal of clinical chemistry, 16 (2013)

[47] Rigon A., Buzzulini F., Soda P., Onofri L., Arcarese L., Iannello G., Afeltra A., Novel opportunities in automated classification of antinuclear antibodies in HEp-2 cells, Autoimmunity Reviews 10 647 –652 (2011)

[48] Sack U., Knoechner S., Warschkau H., Pigla U., Emmrich F., Kamprad M., Computer-assisted classification of HEp-2 immunofluorescence patterns in autoimmune diagnostics, Autoimmunity Reviews, 2 298–304 (2003)

[49] Perner P., Perner H., Muller B., Mining knowledge for Hep-2 cell image classification, Art. Int. Med., 26, 161-173 (2002)

[50] Hiemann R., Hilger N., Michel J., Nitschke J., Böhm A., Anderer U., Weigert M., Sack U., Automatic analysis of immunofluorescence patterns of Hep-2 cells, N.Y. Acad. Sci. 1109, 358–371 (2007).

[51] Sack U., Knoechner S., Warschkau H., Pigla U., Emmrich F., Kamprad M., Computer-assisted classification of HEp-2 immunofluorescence patterns in autoimmune diagnostics, Autoimmunity Reviews, 2, 298–304 (2003)

[52] Progress in Autoimmune Diseases Research, National Institutes of Health, The Autoimmune Diseases Coordinating Committee, Report to Congress

(2005)

[53] Bradwell A. R., Hughes R. G., Atlas of Hep-2 patterns

[54] Quality assurance for the indirect immunofluorescence test for autoantibodies to nuclear antigen (IF-ANA): Approved guideline. NCCLS I/LA2-A, Wayne, PA, 16(11); 1996.

[55] Tozzoli R., Antico A., Porcelli B., Bassetti D., Automation in indirect immunofluorescence testing: a new step in the evolution of the autoimmunology laboratory, Autoimmun Highlights 3:59–65 (2012)

[56] Chiang A., Liu P., Lien Y., Huang Y., Hsieh T., Automatic Detection of Antinuclear Autoantibodies Cells in Indirect Immunofluorescence Images, International Conference on Biomedical Engineering and Informatics (BMEI 2010)

[57] Huang Y., Jao Y., Hsieh T., Chung C., Adaptive Automatic Segmentation of HEp-2 Cells in Indirect Immunofluorescence Images, IEEE International Conference on Sensor Networks, Ubiquitous, and Trustworthy Computing (2008)

[58] Huang Y., Chung C., Hsieh T., Jao Y., Outline Detection for the HEp-2 Cell in Indirect immunofluorescence Images Using Watershed Segmentation, IEEE International Conference on Sensor Networks, Ubiquitous, and Trustworthy Computing (2008)

[59] Percannella G., Soda P., Vento M., A classification-based approach to segment HEp-2 cells, IEEE (2012)

[60] Soda P., Iannello G., ANN-Based Classification of Indirect ImmunoFluorescence Images, World Academy of Science, Engineering and Technology 20 (2006)

[61] Soda P., Iannello G., Vento M., A multiple expert system for classifying fluorescent intensity in antinuclear autoantibodies analysis, Pattern Anal. Applic. 12:215–226 (2009)

[62] Soda P., Early Experiences in the Staining Pattern Classification of HEp-2 Slides, Twentieth IEEE International Symposium on Computer-Based Medical Systems (CBMS'07) (2007)

[63] Soda P., Iannello G., A Hybrid Multi-Expert Systems for HEp-2 Staining Pattern Classification, 14th International Conference on Image Analysis and Processing (ICIAP) (2007)

[64] Soda P., Iannello G., Aggregation of Classifiers for Staining Pattern Recognition in Antinuclear Autoantibodies Analysis, IEEE Transactions On Information Technology In Biomedicine, Vol. 13, No. 3, (2009)

[65] Iannello G., Onofri L., Soda P., A Bag of Visual Words Approach for Centromere and Cytoplasmic Staining Pattern Classification on HEp-2 Images, IEEE (2012)

[66] Hsieh T., Huang Y., Chung C., Huang Y., HEp-2 Cell Classification in Indirect Immunofluorescence Images, ICICS (2009)

[67] Bossuyt X., Cooreman S., De Baere H., Verschueren P., Westhovens R., Blockmans D., Mariën G., Detection of antinuclear antibodies by automated indirect immunofluorescence analysis, Clinica Chimica Acta 415, 101–106 (2013)

[68] Elbischger P., Geerts S., Sander1 K., Ziervogel-Lukas G., Sinah P., Algorithmic Framework For Hep-2 Fluorescence Pattern Classification To Aid Auto-Immune Diseases Diagnosis, ISBI (2009)

[69] Foggia P., Percannella G., Soda P., Vento M., Early Experiences in Mitotic Cells Recognition on HEp-2 Slides, IEEE (2010)

[70] Ersoy I., Bunyak F., Peng J., Palaniappan K., HEp-2 Cell Classification in IIF Images Using ShareBoost, 2012 ICPR

[71] Strandmark P., Ul´en J., Kahl F., HEp-2 Staining Pattern Classification, 2012 ICPR

[72] Li K., Yin J., Lu Z., Kong X., Zhang R., Liu W., Multiclass boosting SVM using different texture features in HEp-2 cell staining pattern classification, ICPR 2012

[73] V. Snell, W. Christmas, J. Kittler, Texture and shape in fluorescence pattern identification for auto-immune disease diagnosis, ICPR 2012

[74] Theodorakopoulos I., Kastaniotis D., Economou G., Fotopoulos S., HEp-2 Cells Classification via Fusion of Morphological and Textural Features,

Proceedings of the IEEE 12th International Conference on Bioinformatics & Bioengineering (BIBE) (2012)

[75] Di Cataldo S., Bottino A., Ficarra E., Macii E., Applying Textural Features to the Classification of HEp-2 Cell Patterns in IIF images, ICPR (2012)

[76] Bel W., Piro P., Giampaglia D., Pourcher T., Barlaud M., Biological cells classification using Bio-Inspired descriptor in a boosting k-NN frame work, IEEE (2012)

[77] Bel W., Giampaglia D., Barlaud M., Piro P., Nock R., Pourcher T., Classification of biological cells using bio-inspired descriptors, ICPR 2012

[78] Ghosh S., Chaudhary V., Feature Analysis for Automatic Classification of HEp-2 Florescence Patterns : Computer-Aided Diagnosis of Auto-Immune Diseases, (ICPR 2012)

[79] Algorithms for clustering data, Jain A., Dubes R., Prentice Hall, 1988

[80] Lee S., Lo C., Wang C., Chung C., Chang C., Yang C., Hsu P., "A computer aided design mammography screening system for detection and classification of microcalcifications", International Journal of Medical Informatics 60, 29-57 (2000)

[81] Huang C., Chung P., Lee T., Yang S., Lee S., Reconstruction and rendering of microcalcifications from two mammogram views by modified projective grid space (MPGS), Computerized Medical Imaging and Graphics 30, 123-133 (2006)

[82] Bhangale T., Desai U. B., Shama U., An unsupervised scheme for detection of microcalcifications on mammograms, IEEE 184-187 (2000)

[83] Sun X., Qian W. ,Song D., Ipsilateral mammogram computer-aided detection of breast cancer, Computerize Medical Imaging and Graphics 28, 151-158 (2004)

[84] Davies D. H., Dance D. R., The automatic computer detection of subtle calcification in radiographically dense breast, Phys. Med. Biol. 37 (6) 1385-1390 (1992)

[85] Hammouda K., Karray F., A comparative study of data clustering techniques, tech. rep., Pattern Analysis and Machine Intelligence Research

Group, University of Waterloo, 2000.

[86] Manuale di diagnostica per immagini, Giorgio Cittadini, ECIG (1995)

[87] Hanley J., McNeil B., The meaning and use of the area under a Receiver Operating Characteristic (ROC) curve, Radiology, 143, 29-36 (1982)

[88] Fawcett T., ROC Graphs: notes and practical consideration for researchers, Kluwer Academic Publishers (2004)

[89] Park S.H., Goo J. M., Jo C., Receiver operating characteristic curve: practical review for radiologists, Korean J. Radiol 5 (1) 11-18 (2004)

[90] Bradley A.P., The use of area under the ROC curve in the evaluation of machine learning algorithms, Pattern Recognition, Vol. 30, No.7, 1145 – 1159 (1997)

[91] Otsu N., A threshold selection method from grey-level histograms, IEEE Transactions On Systems, Man, And Cybernetics, Vol. Smc-9, No. 1 (1979)

[92] Umbaugh Scot E, Computer Vision and Image Processing, Prentice Hall, NJ, (1998)

[93] Report of the First International Contest on HEp-2 Cells Classification, hosted by the 21th ICPR (2012), http://mivia.unisa.it/hep2contest

Acknowledgements

A special thanks goes to Dr. Fabio Bellavia, my personal Matlab trainer, who helped me to solve many problems.

I want to thank some of my friends: Giovanna, Barbara and Adriano for every virtual (and real) coffee and dinner spent together; Maria Rosa and Chiara, for having shared with me their previous PhD experience; Kate, the best English teacher I've ever had.

I thank my family, which supported me especially in the last period.

In my opinion, pursuing a doctorate is not advisable for married couples: it's not easy to bear the pressure and stress deriving from it, so I think my husband should thank me for the patience, the constancy, and the determination with which I faced up this experience (and yes, I know, maybe I should thank him for the same things…).

Finally, I want to thank my daughter: she's still too young but one day I'll tell her how she helped me with her smiles. Actually she is the most beautiful thing happened to me during this PhD.